IRIS AperTO

UNIVERSITÀ DEGLI STUDI DI TORINO

AperTO - Archivio Istituzionale Open Access dell'Università di Torino

Thermal weakening of the carbonate basement under Mt. Etna volcano (Italy): Implications for volcano instability

This is a pre print version of the following article:

Original Citation:

Availability:

This version is available http://hdl.handle.net/2318/121812 since

Published version:

DOI:10.1016/j.jvolgeores.2012.10.004

Terms of use:

Open Access

Anyone can freely access the full text of works made available as "Open Access". Works made available under a Creative Commons license can be used according to the terms and conditions of said license. Use of all other works requires consent of the right holder (author or publisher) if not exempted from copyright protection by the applicable law.

(Article begins on next page)

20 April 2024

Accepted Manuscript

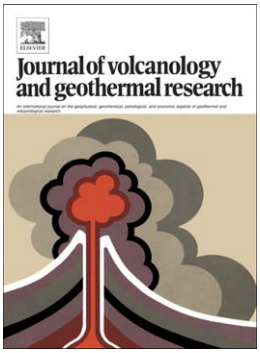

Thermal weakening of the carbonate basement under Mt. Etna volcano (Italy): Implications for volcano instability

M.J. Heap, S. Mollo, S. Vinciguerra, Y. Lavallée, K.-U. Hess, D.B. Dingwell, P. Baud, G. Iezzi

PII: S0377-0273(12)00305-8
DOI: doi: 10.1016/j.jvolgeores.2012.10.004
Reference: VOLGEO 5004

To appear in: *Journal of Volcanology and Geothermal Research*

Received date: 19 April 2011
Accepted date: 9 October 2012

Please cite this article as: Heap, M.J., Mollo, S., Vinciguerra, S., Lavallée, Y., Hess, K.-U., Dingwell, D.B., Baud, P., Iezzi, G., Thermal weakening of the carbonate basement under Mt. Etna volcano (Italy): Implications for volcano instability, *Journal of Volcanology and Geothermal Research* (2012), doi: 10.1016/j.jvolgeores.2012.10.004

This is a PDF file of an unedited manuscript that has been accepted for publication. As a service to our customers we are providing this early version of the manuscript. The manuscript will undergo copyediting, typesetting, and review of the resulting proof before it is published in its final form. Please note that during the production process errors may be discovered which could affect the content, and all legal disclaimers that apply to the journal pertain.

ACCEPTED MANUSCRIPT

Thermal weakening of the carbonate basement under Mt. Etna volcano (Italy): implications for volcano instability

M. J. Heap[1], S. Mollo[2], S. Vinciguerra[3], Y. Lavallée[4], K. -U. Hess[4], D. B. Dingwell[4], P. Baud[1] and G. Iezzi[5]

[1]*Laboratoire de Déformation des Roches, Institut de Physique de Globe de Strasbourg (UMR 7516 CNRS, Université de Strasbourg/EOST), 5 rue René Descartes, 67084 Strasbourg cedex, France.*

[2] *Istituto Nazionale di Geofisica e Vulcanologia. Via di Vigna Murata 605 00143 Rome Italy.*

[3]*Dipartimento di Scienze della Terra, Università di Torino, Via Valperga Caluso 35, 10125, Turin, Italy.*

[4]*Earth and Environment, LMU – University of Munich, Theresienstr. 41/III, 80333 München, Germany.*

[5]*Dipartimento DIGAT, Università G. d'Annunzio, Via Dei Vestini 30, I-66013 Chieti, Italy.*

ACCEPTED MANUSCRIPT

ACCEPTED MANUSCRIPT

Abstract

The physical integrity of a sub-volcanic basement is crucial in controlling the stability of a volcanic edifice. For many volcanoes, this basement can comprise thick sequences of carbonates that are prone to significant thermally-induced alteration. These debilitating thermal reactions, facilitated by heat from proximal magma storage volumes, promote the weakening of the rock mass and likely therefore encourage edifice instability. Such instability can result in slow, gravitational spreading and episodic to continuous slippage of unstable flanks, and may also facilitate catastrophic flank collapse. Understanding the propensity of a particular sub-volcanic basement to such instability requires a detailed understanding of the influence of high temperatures on the chemical, physical, and mechanical properties of the rocks involved. The juxtaposition of a thick carbonate substratum and magmatic heat sources makes Mt. Etna volcano an ideal candidate for our study. We investigated experimentally the effect of temperature on two carbonate rocks that have been chosen to represent the deep, heterogeneous sedimentary substratum under Mt. Etna volcano. This study has demonstrated that thermal-stressing resulted in a progressive and significant change in the physical properties of the two rocks. Porosity, wet (i.e., water-saturated) dynamic Poisson's ratio and wet Vp/Vs ratio all increased, whilst P- and S-wave velocities, bulk sample density, dynamic and static Young's modulus, dry Vp/Vs ratio, and dry dynamic Poisson's ratio all decreased. At temperatures of 800 °C, the carbonate in these rocks completely dissociated, resulting in a total mass loss of about 45% and the release of about 44 wt.% of CO_2. Uniaxial deformation experiments showed that high *in-situ* temperatures (> 500°C) significantly reduced the strength of the carbonates and altered their deformation behaviour. Above 500 °C the rocks deformed in a ductile manner and

ACCEPTED MANUSCRIPT

the output of acoustic emissions was greatly reduced. We speculate that thermally-induced weakening and the ductile behaviour of the carbonate substratum could be a key factor in explaining the large-scale deformation observed at Mt. Etna volcano. Our findings are consistent with several field observations at Mt. Etna volcano and can quantitatively support the interpretation of (1) the irregularly low seismic velocity zones present within the sub-volcanic sedimentary basement, (2) the anomalously high CO_2 degassing observed, (3) the anomalously high Vp/Vs ratios and the rapid migration of fluids, and (4) the increasing instability of volcanic edifices in the lifespan of a magmatic system. We speculate that carbonate sub-volcanic basement may emerge as one of the decisive fundamentals in controlling volcanic stability.

Keywords: Mt. Etna; temperature; carbonate basement; decarbonation; strength; ultrasonic wave velocities, elastic moduli; Vp/Vs ratio; CO_2 budget; X-ray powder diffraction; thermo-gravimetric analysis; microstructure

ACCEPTED MANUSCRIPT

ACCEPTED MANUSCRIPT

1. Introduction

The stability of a volcanic edifice is a significant element of risk assessment (McGuire, 1996). Volcanoes, built from successive eruptions, effusive or explosive, can be depicted as pseudo-stable piles of rocks. In contrast to non-volcanic mountains, which form by very slow uplift, volcanoes are built rapidly and heterogeneously, both in time and space. One clear consequence is their high propensity for mass wasting. Volcanic edifice instability need not "merely" result in the slow, gravitational spreading and episodic to continuous slippage of unstable flanks, but can also encourage instantaneous and devastating flank collapse (Siebert, 1992). Field surveys worldwide have shown that the collapse of volcanic flanks is common, if not ubiquitous in the prolonged lifetime of a volcano (Davidson and De Silva, 2000). The consequences of such events can be enormous, both in humanitarian and in economic terms. The integrity of the sub-volcanic basement (the foundation on which the pseudo-stable volcanic pile rests) must therefore be of paramount importance in volcano stability. Previous studies have indeed highlighted the importance of the sub-volcanic basement in edifice stability (Van Wyk De Vries and Borgia, 1996; McGuire, 1996; Van Wyk De Vries and Francis, 1997; Szakács and Krézsek, 2006). Unfortunately (in terms of stability), as is the case for many high-risk, active volcanoes, when the sub-volcanic basement is comprised of thick carbonate sequences it is prone to thermally-induced reactions. Heat, provided by magmatic activity (e.g., see Bonaccorso *et al.*, 2010), can result in detrimental mineralogical, chemical, and textural modifications to carbonate rock, leaving it intensely altered, fractured, and thus weakened (e.g., Homand-Etienne and Troalen, 1984; Samtani *et al.*, 2002; Chen *et al.*, 2009; Mao *et al.*, 2009). The presence of large, sub-volcanic carbonate sedimentary successions within volcanic systems is common. Sub-volcanic

ACCEPTED MANUSCRIPT

carbonate basements seen at high-risk volcanoes worldwide: Mt. Etna volcano (e.g. Lentini, 1982; Grasso and Lentini, 1982; Pedley and Grasso, 1992), Mt. Vesuvius (Bruno *et al.*, 1998; Iacono-Marziano *et al.*, 2009), the Colli Albani volcanic district (Chiodini and Frondini, 2001; Iacono-Marziano *et al.*, 2007; Freda *et al.*, 2008; Gaeta *et al.*, 2009; Mollo *et al.*, 2010a) and the Campi Flegrei volcanic district (D'Antonio, 2011) in Italy, Popocatépetl volcano (Goff *et al.*, 2001) and the Colima volcanic complex (Norini *et al.*, 2010), both Mexico, Yellowstone volcanic system, USA (Werner and Brantley, 2003) and Merapi, Indonesia (Chadwick *et al.*, 2007; Deegan *et al.*, 2010; Troll *et al.*, 2012). It becomes clear therefore, that an important element of volcano stability must focus on the understanding of the potential thermally-induced weakening of rock representative of the carbonate successions present under active volcanoes.

In this study, we used Mt. Etna (Italy), the largest volcanic edifice in Europe (40 km wide and standing 3.3 km above sea level), as a case study. Mt. Etna volcano represents an ideal candidate for our study. Firstly, Mt. Etna is one of the most intensively monitored volcanoes on Earth. Over the last 20 years, new technological developments and denser monitoring networks at Mt. Etna have provided one of the highest quality volcanological, geophysical, and geochemical datasets available for any volcano in the world (Bonaccorso, 2004; Acocella and Puglisi, 2012). Studies have shown that there is a continuous large-scale ESE seaward sliding of the eastern flank of Mt. Etna (e.g., Borgia *et al.*, 1992; Borgia *et al.*, 2000; Bonforte and Puglisi, 2003; Rust *et al.*, 2005; Bonforte and Puglisi, 2006; Palano *et al.*, 2008; Palano *et al.*, 2009), with an average rate, calculated from geodetic data collected at the Pernicana fault since 1997, of about 2.8 cm/year (Azzaro *et al.*, 2001; Palano *et al.*, 2009). A large décollement surface, potentially dictating this large-scale deformation by driving gravity-driven edifice spreading, has been

ACCEPTED MANUSCRIPT

inferred to exist either at a depth of about 5 km (e.g., Froger *et al.*, 2001; Neri *et al.*, 2004; Lundgren *et al.*, 2004) or at a depth between 1.5 and 3 km (e.g., Bonforte and Puglisi, 2003; Palano *et al.*, 2008).

Secondly, the thin (about 1.5 km thick) basaltic cover at Mt. Etna volcano rests upon a vast sub-volcanic sedimentary basement, comprising of a melange of marly clays, marly limestones and quartz-arenitic rocks (about 2 km thick, see Catalano *et al.*, 2004) from the Maghrebian-Appennine Chain, that overly a thick Mesozoic to Mid-Pleistocene carbonate succession of limestone and dolomite, referred to as the Hyblean Plateau, or Iblean Plateau (Lentini, 1982; Grasso and Lentini, 1982; Pedley and Grasso, 1992). The Hyblean Plateau is inferred to start at about a depth of 5 km underneath the volcanic edifice (Tibaldi and Groppelli, 2002; Behncke and Neri, 2003; Lundgren *et al.*, 2004; Andronico *et al.*, 2005) and has an average thickness of about 10 km (see Yellin-Dror *et al.*, 1997 and references therein). Importantly, large, long-lived magma bodies are known to be present at depths corresponding to the Hyblean Plateau, as inferred by P-wave inversion tomography (Chiarabba *et al.*, 2000), thermo-mechanical numerical modelling (Del Negro *et al.*, 2009; Bonaccorso *et al.*, 2010), and *b*-value mapping (Murru *et al.*, 1999). However, the involvement of the Hyblean Plateau with the magmatic plumbing system at Mt. Etna volcano does not end there, as new heat sources, in the form of eccentric reservoirs or peripheral dykes that have fed recent flank eruptions, are also inferred to populate these depth intervals (Behncke and Neri, 2003; Acocella and Neri, 2003; Andronico *et al.*, 2005; Carbone *et al.*, 2009; Bonforte *et al.*, 2009), thus possibly exposing fresh, unaltered carbonate rock to high temperatures. Volcanic activity at the flanks of Mt. Etna during the 2001 eruptions (Acocella and Neri, 2003; Behncke and Neri, 2003) was considered to involve the emplacement of a shallow

ACCEPTED MANUSCRIPT

dyke (Bonaccorso *et al.*, 2002; Patanè *et al.*, 2002) at about 3.5 km depth; however, structural and seismic evidence exclude a shallow connection between the summit and the peripheral magmatic systems (Acocella and Neri, 2003). Since the connection between the summit and the peripheral magmatic systems is considered to be at deeper crustal levels (Acocella and Neri, 2003; Carbone *et al.*, 2009), the peripheral dykes are likely to have traversed through rocks of the Hyblean Plateau previously unexposed to high temperatures. This was supported by the fact that, not only was the magma erupted at the flank chemically distinct from that from the summit, but it also contained abundant sedimentary (mostly calcarenites and sandstones) inclusions (Behncke and Neri, 2003). It was therefore postulated that a new eccentric reservoir, located within the Hyblean Plateau, fed these new flank eruptions (see Fig. 8 in Behncke and Neri, 2003). The 2002-2003 flank eruptions at Mt. Etna volcano were characterised by continuous explosive activity and intermittent lava extrusion, involving the opening of fissures on the north-eastern and southern flanks (Andronico *et al.*, 2005). The magma erupted from the southern fissure during 2002-2003 was found to be similar in composition to that erupted in 2001, and also contained sedimentary xenoliths. It is believed that the 2002-2003 eruptions were fed by the same eccentric reservoir exploited in 2001 (Andronico *et al.*, 2005), albeit the magma travelled to the surface using a new route. Although the lithology of the majority of the erupted xenoliths (in 2001 and 2002-2003) matched more closely with the sediments of the Maghrebian-Appennine Chain, we contend that such renewed activity at depth could have exposed fresh, unaltered carbonate rock of the Hyblean Plataeu to high temperatures. More recently, there was activity renewed at Mt. Etna between 2008-2009 (see Alparone *et al.*, 2012 and references therein). Although, evidence suggests that, although a new dyking mechanism may be

ACCEPTED MANUSCRIPT

responsible, it would be too shallow to create any new pathways through the Hyblean Plateau (Aloisi *et al.*, 2009).

The geochemical signature of magma-carbonate interaction can sometimes be seen within volcanic products, and is known as "carbonate assimilation" (e.g., Wenzel *et al.*, 2002; Barnes *et al.*, 2005; Gaeta *et al.*, 2006; Piochi *et al.*, 2006; Chadwick *et al.*, 2007; Freda *et al.*, 2008; Deegan *et al.*, 2010; Mollo *et al.*, 2010a). Recent petrological studies have documented in detail that magma contamination is marked by the overgrowth of Ca-rich phases (mainly calcic clinopyroxene) on primary minerals (essentially olivine); as a result, the magma becomes progressively depleted in silica and enriched in alkalis. This results in the release of CO_2 and Ca-rich fluids (Ague, 2003) that are strongly controlled by the development of permeability within the rocks (Balashov and Yardley, 1998; Buick and Cartwright, 2000). Recently, Gaeta *et al.* (2009) and Mollo *et al.* (2010a) have provided new insights into the large-scale, magma-carbonate interaction processes occurring in magma chambers during magmatic contamination and differentiation. Mollo *et al.* (2010a) proposed that carbonate assimilation is a three-phase (solid, melt, and fluid) process whose main products are: diopside-CaTs clinopyroxene solid solution, silica-undersaturated CaO-Al_2O_3-rich melt, and C–O–H fluid phase. Whereas, Gaeta *et al.* (2009) showed that magmatic skarns formed at the magma-carbonate interface, act as a source of CaO-Al_2O_3-rich silicate melt and that the assimilation of this melt is the process responsible for magma contamination, rather than the ingestion of carbonate wall-rocks. However, whereas some evidence for the proximity of the carbonate basement to the magma sources at Mt. Etna have been provided in the form of: (1) variably-altered carbonate xenoliths, considered to be derived from the limestones and dolomites from the Monte Judica formation

ACCEPTED MANUSCRIPT

and the Hyblean Foreland Units, found within lavas erupted in 1892, 1986, and within the persistent activity of 1989 at Bocca Nuova (Michaud, 1995); (2) abundant sedimentary xenoliths found in lavas of the July–August 2001 eruption (Behncke and Neri, 2003) and the magma erupted from the southern fissure during 2002-2003 (Andronico *et al.*, 2005); and (3) geological and structural evidence (Grasso and Lentini, 1982; Lentini, 1982), as well as the geophysical evidence outlined above, petrological data excludes the ingestion and assimilation of carbonate materials in magmas at Mt. Etna volcano. The lavas expelled from Mt. Etna volcano in the last 300 ka are of alkaline affinity and range from hawaiite to benmoreite in composition (Tanguy *et al.*, 1997). Plagioclase, clinopyroxene, olivine, and titanomagnetite are common minerals for the majority of historical and pre-historical products. Several experimental studies have demonstrated that the liquid line of descent of Etnean magmas is related to the crystallization of these mineral phases under both equilibrium and disequilibrium conditions (Métrich and Rutherford, 1998; Del Gaudio *et al.*, 2010; Mollo *et al.*, 2010b; Mollo *et al.*, 2011b). However, in a recent study, it has been suggested that the carbon isotope variations in degassed volcanic CO_2 at Mt. Etna could be due to carbonate assimilation (Chiodini *et al.*, 2011). While the petrological implications of magma-carbonate interaction processes is not the goal of this study, when mantle-derived melts interact with the crust, a "non-eruptible" magmatic zone (i.e., a solidification front close to the carbonate wall-rocks) may form between the large magmatic bodies and the host rock (Marsh, 1995). Under such circumstances, it is still unclear to what extent crustal materials may affect the original composition of magmas (c.f., Mollo *et al.*, 2010c); this case likely applies to low-temperature (< 1100 °C) trachybasaltic liquids that are erupted from Mt. Etna volcano (c.f. Mollo et al., 2011b) as these crystallize readily. It must be noted that, although our study reports such changes under ambient pressure conditions (i.e.,

ACCEPTED MANUSCRIPT

without confinement), it has been demonstrated that, at magmatic temperatures and pressures, carbonate inevitably dissociates (Freda *et al.*, 2008; Mollo *et al.*, 2010a).

The irrevocable fact remains that the carbonate rocks present under Mt. Etna will be exposed to high temperatures as a result of their proximity to large, long-lived magmatic bodies (Murru *et al.*, 1999; Chiarabba *et al.*, 2000; Bonaccorso *et al.*, 2010), and lateral growth of the reservoir via eccentric dyking and ponding (Carrigan *et al.*, 1992; Behncke and Neri, 2003; Acocella and Neri, 2003; Andronico *et al.*, 2005; Carbone *et al.*, 2009; Bonforte *et al.*, 2009), as well as circulating hot fluids (Siniscalchi *et al.*, 2010): "proximity without intimacy". Indeed, accelerated flank movements are commonly observed to follow magmatic events within the sedimentary substratum (Walter *et al.*, 2005), highlighting the intimate link between basement deformation and flank instability. Fig. 1 shows a schematic of Mt. Etna volcano (redrawn from Tibaldi and Groppelli, 2002) that illustrates the juxtaposition of the deep carbonate substratum and the magmatic heat sources.

Recent experimental work has focussed on quantifying the evolution of the physical and mechanical properties of Etnean surficial basaltic rocks under both mechanical and thermal stresses (Balme *et al.*, 2004; Rocchi *et al.*, 2004; Vinciguerra *et al.*, 2005; Stanchits *et al.*, 2006; Benson *et al.*, 2007; Benson *et al.*, 2008; Heap *et al.*, 2009; Fortin *et al.*, 2010; Heap *et al.*, 2011). However, the relative importance of the sub-volcanic sedimentary basement is reinforced by the fact that reconstructions of the morphology of Mt. Etna volcano reveal only about 373 km^3 of the bulk total volume of about 1400 km^3 is comprised of volcanic rocks (Catalano *et al.*, 2004 and references therein). The remaining 1027 km^3 is composed of sediments of the

ACCEPTED MANUSCRIPT

Maghrebian-Appennine Chain and the carbonate successions of the Hyblean Plateau (Catalano *et al.*, 2004). Mollo *et al*. (2011a) experimentally investigated the physical and mechanical properties of a marly limestone from the Maghrebian-Appennine Chain (from the Sicilide Unit). The rock was chosen to represent these shallow sediments and is composed of 75% calcite, 15% quartz and 10% kaolinite, and contains a porosity of 2.5%. They found that the samples were severely weakened upon exposure to 760 °C, a result of devolatilization reactions (i.e., clay dehydroxylation and calcite decarbonation). In contrast, complementary experiments on basaltic rocks did not display any thermally-induced weakening (Mollo *et al.*, 2011a). Mollo *et al*. (2012) recently extended this study by performing decarbonation experiments within a "closed" system (i.e., buffered by CO_2 to inhibit decarbonation). Their experiments showed that, even when decarbonation is halted, rock physical properties still degrade due to thermal microcracking. They concluded that (1) due to the porous and permeable nature of a volcanic edifice, a "closed" system may be unrealistic; further, the thermal microcracks that would form in the absence of decarbonation may also provide routes for the escape of CO_2 and, (2) as a result, the generation of CO_2 via decarbonation is unlikely to hinder its impact on volcano instability (Mollo *et al.*, 2012).

To complement the data of Mollo *et al*. (2011a; 2012), we have conducted a detailed study of the influence of high temperature (up to 800 °C) on the physical (e.g., porosity, ultrasonic wave velocities, and elastic moduli), chemical (e.g., compositional changes) and mechanical properties of two carbonate rocks containing a high (>95 wt.%) carbonate content (one of 100 wt.% calcite and the other 78 wt.% calcite and 22 wt.% dolomite), specifically chosen to span the heterogeneity within the limestone and dolomite lithological successions of the Hyblean Plateau

ACCEPTED MANUSCRIPT

underneath Mt. Etna volcano. The maximum experimental temperature of 800 °C represents our predicted (based on standard heat conduction theory, see Carslaw and Jaeger, 1986; see also Carrigan *et al.*, 1992; Bonaccorso *et al.*, 2010) upper boundary for the carbonates of the Hyblean Plateau. In practice, this may only represent the volume at the margins of magmatic bodies and dykes (although this volume may be significant). Our data aim to provide a complete range for the expected temperature-induced changes for the carbonates comprising the Hyblean Plateau. Below we introduce the investigated materials and explain the experimental techniques. Next, we present the extent of the chemical, physical and mechanical property changes with thermal-stressing for both carbonates. We flank these data by providing microstructural observations before and after thermal-stressing and a CO_2 budget for carbonate basement decarbonation at Mt. Etna. Finally, we discuss the results in terms of their implications for the stability and the interpretation of geophysical anomalies/observations at Mt. Etna volcano.

2. Material characterisation and experimental methodology

2.1 Experimental materials

The two carbonates chosen to span the heterogeneity within the Hyblean Plateau below Mt. Etna volcano were: (1) Mt. Climiti limestone (MCL), thick-bedded bio-calcarenites units in the Monti Climiti Formation of the Sortino Group in Southeast Sicily (Italy) (Pedley, 1981; Grasso and Lentini, 1982) and, (2) Thala limestone (TL), a micritic limestone from the Abiod limestones of Northwest Tunisia (Burollet, 1991). Their “as-collected” (i.e., before any thermal-stressing or deformation) chemical and physical properties are summarised in Tables 1 and 2, respectively

ACCEPTED MANUSCRIPT

(the methods used to ascertain these values are described below). Noteworthy differences between the selected rock types include: (1) the presence versus absence of dolomite, (2) their connected porosity (TL = 18.4% and MCL = 25.2%) and, (3) their unconfined compressive strengths (UCS).

2.2 Chemical analyses

2.2.1 "As-collected" chemical analysis

"As-collected" bulk rock compositions were analysed at the Activation Laboratories Ltd (Ontario, Canada) using a Spectro CIROS inductively coupled plasma-atomic emission spectrometer (ICP-AES). For the ICP-AES analyses, the powdered samples were mixed with a flux of lithium metaborate and lithium tetraborate, and then fused in an induction furnace at a temperature of 1100 °C.

2.2.1 Methods to track thermally-induced chemical changes

Thermo-gravimetric (TG) and scanning differential calorimetry (DSC) analyses were carried out using a Netzsch STA 449 C thermobalance apparatus. Powdered samples (of approximately 40 mg) were heated in a static air atmosphere in a platinum crucible (with lid) at a heating rate of 10 °C/min up to a temperature of 100 °C. The samples were then maintained at 100 °C for 60 minutes to ensure that the sample was completely dry of atmospheric moisture. Samples were then heated to a target temperature of 1000 °C, again at 10 °C/min. The mass loss and heat flow,

ACCEPTED MANUSCRIPT

monitored during heating, were used to track the temperatures at which calcite and dolomite dissociate.

The mass-loss-on-calcination, calcimetry, and X-ray powder diffraction (XRPD) analyses were performed on powdered MCL and TL samples that were either maintained at ambient temperature or thermally-stressed to pre-determined temperatures of 200, 400, 500, 600, 650, and 800 °C. Mass-loss-on-calcination analysis was performed in a Nabertherm LHT 04/18 chamber furnace at the HP-HT Laboratory of the Istituto Nazionale di Geofisica e Vulcanologia (INGV, Rome, Italy). For each thermal-stressing temperature, 5 g of powdered sample was heated at a rate of 10 °C/min to a target temperature of 1200 °C. The samples were then held at that temperature for duration of 12 hours, to ensure complete decarbonation, and the loss of mass was measured. Calcimetry analysis was performed using a Dietrich-Frühling calcimeter at the Dipartimento di Scienze Geologiche of the University "Roma Tre" in Rome. For each thermal-stressing temperature, 1 g of powdered sample was dissolved in 15 ml of 6 N hydrochloric acid (density = 1.12 $g.cm^{-3}$) and the volume of CO_2 released was measured.

XRPD analyses were performed using the Siemens D-5005 diffractometer at the DIGAT department, Università G. d'Annunzio of Chieti (Italy). It operates in the vertical θ-2θ Bragg-Brentano configuration and is equipped with a Ni-filtered Cu*K*α radiation. All data were collected in the 2θ range of 3° to 70°, with a step scan of 0.02° and a counting time of 8 seconds per step. For each analysis, 10 mg of sample was powdered in alcohol and then mounted into the central hole (10 x 10 x 0.5 mm) of a nominally zero-background Si-sample holder (Li and Albe, 1993). The identification of crystalline phases for each pattern was performed by comparison

ACCEPTED MANUSCRIPT

with crystal models reported in the commercial Inorganic Crystal Structure Database (ICSD), thus allowing a fit to the observed Bragg reflection (2θ positions and relative intensities). For each crystalline compound identified, the lattice parameters, atomic positions, and space groups were then used for the successive Le Bail and Rietveld refinements (Young, 1993; Le Bail, 2005; Percharsky and Zavaliji, 2005), both implemented in the EXPGUI-GSAS software package (Larson and von Dreele, 1997; Toby, 2001). For the former refinement method, the background was initially constrained manually and subsequently modelled by a polynomial Chebyshev function using five to ten coefficients. Then, cell parameters for each crystalline phase and a constrained sample displacement parameter were refined. Bragg peak profiles were modelled using the function refining both Lorentzian (Lx, Ly) and Gaussian (GW) contributions (Finger *et al.*, 1994). Each Le Bail refinement was terminated when the observed XRPD spectra were adequately reproduced. All these parameters were then kept fixed and used in the following Rietveld refinement, where only the scale factor was refined to obtain a Quantitative Phase Analysis (QPA).

2.3 Physical property analyses

2.3.1 "As-collected" physical property analysis

UCS experiments were performed on "dry" (used to describe samples that have been at 40 °C in a vacuum oven for at least 24 hours, and were deformed under "ambient humidity" conditions) cylindrical samples, 20 mm in diameter and 40 mm in length, using the uniaxial press at the Laboratoire de Déformation des Roches (LDR, Université de Strasbourg, Fig. 2A). Samples were

ACCEPTED MANUSCRIPT

loaded at a constant strain rate of 1.0×10^{-5} s^{-1} until failure. Axial strain was continuously monitored during experimentation by means of an LVDT transducer. The output of AE energy was monitored throughout via a piezoelectric transducer (located within the bottom anvil) with a high response band over the range 100 kHz – 1MHz. AE signals were recorded by a Physical Acoustics USB AE Node at a sampling rate of 10 MHz. The signal threshold was set at 30 dB. After each experiment, we computed the cumulative output of AE energy as a function of strain or displacement, and the evolution of the analogue seismic *b*-value. The seismic *b*-value is the negative slope of the log-linear AE amplitude-frequency distribution (Gutenberg and Richter, 1955; Gutenberg and Richter, 1956) here calculated using Aki's maximum likelihood method (Aki, 1965) for every 200 AE hits at 100 hit intervals. Since the *b*-value describes the amplitude-frequency distribution of AE hits during a deformation process, it has also been interpreted as describing the size-frequency distribution of cracking events in rock deformation (Main *et al.*, 1989; Meredith *et al.*, 1990). In particular, a decrease in the *b*-value as the level of stress is increased has been interpreted as a change from distributed, small-scale cracking at low stress to more localized, larger-scale cracking in the approach to failure at high stress (Meredith *et al.*, 1990; Sammonds *et al.*, 1992; Smith *et al.*, 2009).

Static Young's moduli were then calculated following the method of Heap and Faulkner (2008). First, the stress-strain curves were fitted with a third-order polynomial in order to ascertain the extent of the linear elastic portion of each curve. The resultant equations were then differentiated and the slopes of the stress-strain curves (i.e., the Young's modulus) determined over their entire lengths (Heap and Faulkner, 2008). The Young's modulus was taken from the linear regions of such curves (i.e., those regions where the moduli did not change). We note that this only

ACCEPTED MANUSCRIPT

represents one Young's modulus in a deforming rock sample, since the elastic moduli will be developing in an anisotropic manner.

Dry and "wet" (used to describe samples that have been vacuum saturated with distilled water) ultrasonic wave velocity measurements were measured on cylindrical samples (20 mm in diameter and 40 mm in length) at the LDR (Université de Strasbourg) using an Agilent Technologies DSO5012A digital storage oscilloscope, an Agilent Technologies 33210A, 10 MHz function/waveform generator and two broadband PZT piezoelectric transducer crystals (100 kHz to 1 MHz frequency) located at the top and bottom of the sample. All measurements were collected under a force of 600 N to ensure a good contact between the endcaps and the sample. Dynamic Young's modulus and Poisson's ratio were then calculated from the resultant elastic wave velocities using the following formulae:

$$\text{Young's modulus } (E_d) = \rho((Vs^2(3Vp^2 - 4Vs^2))/(Vp^2 - Vs^2)) \quad (1)$$

$$\text{Poisson's ratio } (v_d) = (Vp^2 - 2Vs^2)/(2(Vp^2 - Vs^2)) \quad (2)$$

Where ρ is the bulk sample density and Vp and Vs are the velocities of compressive and shear waves, respectively.

2.3.2 Methods to track thermally-induced physical property changes

ACCEPTED MANUSCRIPT

UCS experiments at high *in-situ* temperatures were performed on the high-temperature uniaxial press at the Ludwig-Maximilians University (LMU), in Munich (Fig. 2B, see also Hess *et al.*, 2007 for details). Experiments were performed on dry, cylindrical samples cored to a diameter of 25 mm and cut parallel to a length of 60 mm. During experimentation, axial strain was measured using an LVDT embedded within the servo-cylinder, and the output of AE was monitored throughout using a PC1-2 based MISTRAS using the same type of transducer described above, set at a signal threshold of 50 dB. Constant strain rate (1.5×10^{-5} s^{-1}) experiments were then performed on samples of both TL and MCL at temperatures of 500, 600, 650, and 800 °C. These temperatures were specifically chosen to investigate (1) the change in strength of the carbonates at approximately the initiation temperature for decarbonation (650 °C) and at a temperature were the rock should be greatly affected by decarbonation reactions (800 °C), as indicated by our TGA data (see section 3.1.2), (2) the brittle-ductile transition (i.e., the switch in behaviour from the sample losing its ability to resist load during strain accumulation, to the rock sustaining strain without losing its ability to resist load, see Rutter, 1986) and, (3) the seismic-aseismic transition (monitored using AE as a proxy).

P-wave velocities were measured at high *in-situ* temperatures using a servo-controlled, uniaxial press equipped with a high-temperature (1200 °C) ceramic fibre furnace at the HP-HT Laboratory (INGV, Rome, Italy). Experiments were performed on dry, cylindrical samples cored to a diameter of 25 mm and cut parallel to a length of 60 mm. Measurements were made on samples at *in-situ* furnace temperatures of 200, 400, 500, 600, 650, and 800 °C. Samples were first loaded to 1 MPa axial load to ensure a good contact between the sample and the pistons, and then heated at a constant heating rate of 10 °C/min to their target temperature. Ultrasonic wave

ACCEPTED MANUSCRIPT

velocities were then measured with a Tektronix DPO4032 digital oscilloscope, using a high voltage (1000 V) pulse generator and two broadband PZT piezoelectric transducer crystals (100 kHz to 1 MHz frequency) located at the top and bottom of the sample. Since S-wave velocities could not be measured at *in-situ* temperatures in our apparatus, in this study we only show *in-situ* measurements for P-wave velocities.

P- and S-wave velocities were also measured at ambient temperature on dry and wet, thermally-stressed samples (i.e., samples that were heated, cooled, and then measured at ambient temperatures) at the LDR (Université de Strasbourg), using the same method described above (see section 2.3.1). For these measurements, samples (20 mm in diameter and 40 mm in length) were either maintained at ambient temperature or thermally-stressed to pre-determined temperatures of 100, 200, 400, 500, 600, 650, 700, and 800 °C at a constant heating and cooling rate of 1 °C/min. Dynamic Young's modulus and Poisson's ratio were then calculated for each thermal-stressing temperature from the resultant elastic wave velocities using equations (1) and (2). Prior to and following thermal-stressing, the connected porosity for each sample was measured using the triple weight (Archimedes) water saturation technique. The total porosity change was also measured for each sample using a helium pycnometer (AccuPyc II 1340 helium pycnometer). In addition, since MCL is essentially 100 wt.% calcite, we were also able to calculate the total porosity of MCL using the bulk sample densities, and assuming the density of calcite to be 2.71 $g.cm^{-3}$ (see Guéguen and Palciauskas, 1994).

Constant strain rate UCS experiments were performed on dry, thermally-stressed samples (the same temperatures listed above) at room temperature using the uniaxial press at the LDR

ACCEPTED MANUSCRIPT

(Université de Strasbourg, Fig. 2A). Samples were loaded at a constant strain rate of 1.0×10^{-5} s^{-1} until failure. Axial strain was continuously monitored during experimentation by means of an LVDT transducer. The output of AE energy was monitored throughout via a piezoelectric transducer located within the bottom anvil (set at the same settings as described for the above room temperature UCS experiments, see section 2.3.1) and recorded using a Physical Acoustics USB AE Node. Static Young's moduli were then calculated from the resultant stress-strain curves using the method outlined above (see section 2.3.1).

Finally, microstructural observations on both "as-collected" samples of MCL and TL and those thermally-stressed to 800 °C (at 1 °C/min) were performed using the JEOL-JSM6500F Field Emission Gun - Scanning Electron Microscope (FE-SEM) located at the HP-HT Laboratory in Rome (INGV).

3. Results

3.1 Results of chemical analyses

3.1.1 "As-collected" chemical composition

"As-collected" chemical compositions for both TL and MCL, measured by ICP-AES, can be found in Table 1. Importantly, the chemical analysis of the carbonates showed that TL contained 22 wt.% of dolomite and 78 wt.% of calcite and that MCL contained 100 wt.% of calcite.

ACCEPTED MANUSCRIPT

3.1.2 Thermal decomposition of carbonate

TG (solid lines) and DSC (dashed lines) curves for MCL and TL are presented in Fig. 3. The curves show that a major mass loss took place in the temperature range of 680-882 °C and 560-905 °C for MCL (Fig. 3A) and TL (Fig. 3B), respectively. The measured mass loss in these ranges corresponds to the CO_2 released during the thermal decomposition of carbonates (i.e., just calcite in the case of MCL and both calcite and dolomite in the case of TL). A minor mass loss was also detected for the two samples in the temperature range 100-120 °C and is most likely attributable to the chemically bound water present in carbonate material (see also Gunasekaren and Anbalagan, 2007), this can be most easily seen as an endothermic peak in the DSC curves (note: samples were kept at 100 °C for 60 minutes prior to heating). The total measured percentage of mass loss was 44 and 45 wt.% for MCL and TL, respectively.

The onset of thermal decomposition of calcite and dolomite can be best observed in the DSC curves. For MCL, the curves show that the calcite started to decompose at temperatures above 680°C, showing a strong endothermic peak at 860 °C (Fig. 3A). The calcite dissociated according to the following reaction (see also Samtani *et al.*, 2002):

$$CaCO_3(s) \rightarrow CaO(s) + CO_2(g) \qquad (3)$$

The thermal decomposition of the calcite therefore produced lime, a CaO solid phase, plus a CO_2 gas phase. However, TL consists of both calcite (78 wt.%) and dolomite (22 wt.%) and, in this case, the decrease in mass initiated at a lower temperature of 560 °C. In case of TL, three

ACCEPTED MANUSCRIPT

endothermic peaks were observed: two endothermic peaks at 775 °C and 810 °C (see the inset in Fig. 3B), seen within the temperature ranges of 756–786 °C and 793–826 °C, respectively, and a third, larger peak at 886 °C. The first two peaks are due to the dissociation of the 22 wt.% of dolomite present in TL. Two peaks were observed since dolomite thermal dissociation is a two-stage decomposition process involving the following reactions (McIntosh *et al.*, 1990; Maitra *et al.*, 2005):

$$CaMg(CO_3)_2(s) \rightarrow CaCO_3(s) + MgO(s) + CO_2(g) \quad (4)$$

The solid calcite products of reaction (4) are then broken down as per reaction (3). Therefore, the complete thermal decomposition of dolomite can be rewritten to:

$$CaMg(CO_3)_2(s) \rightarrow MgO(s) + CaO(s) + 2\ CO_2(g) \quad (5)$$

The thermal decomposition of the dolomite therefore produced periclase, a MgO solid phase, a lime solid phase, plus a CO_2 gas phase. In Fig. 3B, the lower temperature peak at 775 °C represents the formation of $CaCO_3$ + MgO according to reaction (4) and the higher peak at 810 °C represents the decomposition of newly-formed calcite following reaction (3). The complete thermal decomposition of dolomite only occurs when its rhombohedral crystal lattice is converted to the cubic lattice of CaO + MgO oxides. The thermal ranges of dolomite decomposition from this study strictly agree with those measured by previous authors (Li and Messing, 1983; McClauley and Johnson, 1991; Kök and Smykatz-Kloss, 2001; Gunasekaren and Anbalagan, 2007). The third peak at 886 °C in the DSC curve represents the decomposition of 78

ACCEPTED MANUSCRIPT

wt.% of calcite (Fig. 3B) according to reaction (3). The largest of the three endothermic peaks is associated with the decomposition of calcite, in agreement with the higher wt.% of calcite in TL with respect to dolomite. It is worth emphasising that the thermal decomposition of dolomite occurred at a lower temperature range than for calcite. This has been previously attributed to the lower strength of the Mg-O bonds in structure of dolomite with respect to the Ca-O bonds in calcite (see Samtani *et al.*, 2002; Gunasekaren and Anbalagan, 2007).

3.1.3 Mineralogical changes during thermal-stressing

The mineralogical changes associated with increasing temperature were monitored by XRPD analysis of "as-collected" and thermally-stressed samples of MCL and TL (Fig. 4). Results show that, at 800 °C, calcite (labelled Cc on Fig. 4) and dolomite (Dm) were completely dissociated according to reactions (3) and (5) discussed above. The XRPD data also showed that portlandite (Pt), $Ca(OH)_2$, appeared in samples thermally-stressed to temperatures above 600 °C (Fig. 4). Portlandite, a calcium hydroxide, forms by the recombination of CaO with atmospheric water vapour by the reaction:

$$CaO + H_2O \rightarrow Ca(OH)_2 \qquad (6)$$

The portlandite must have formed after the samples thermally-stressed to 800 °C (and 650 °C in the case of MCL) had cooled, when water became readily available in the atmosphere. The reaction is exothermic and results in a considerable volume increase (Boynton, 1980). In fact, the dramatic sample volume increase, as a result of portlandite formation, severely afflicted the

ACCEPTED MANUSCRIPT

samples. Some samples disintegrated on touch, whilst others even "exploded" on the benchtop. At 800 °C, lime (Li) and periclase (Pe) were also observed as final solid products of calcite and dolomite dissociation. The amount of CO_2 released from the samples during the decarbonation process is displayed in Fig. 3; the decreasing carbonate content is also reported for comparison. The results are qualitatively similar to the TG/DSC data of Fig. 3: changes start to occur at temperatures about 600 °C and progress rapidly as temperature is further increased. Fig. 5 shows that, at 800 °C, the carbonate minerals were completely dissociated, in agreement with the XRPD analysis, and that their dissociation produced about 44 wt.% of CO_2 in both MCL and TL. It is interesting to note that, although the samples contained different quantities of calcite and dolomite, their total wt.% of released CO_2 were essentially identical, in accordance with the stoichiometry of the mineral phases.

3.1.4 Microstructural observations

FE-SEM compositional photomicrographs of samples of MCL and TL, on "as-collected" samples and samples thermally-stressed to 800 °C, are shown in Fig. 6. Both MCL and TL show clear mineralogical, textural, and structural differences due to the influence of high temperature. At 800 °C, the porosity (in black) can be seen to be greatly increased in both samples. In MCL, the pervasive thermal microcracks within the lime crystals form a mosaic pattern (see inset on Fig. 6D). The lime crystals also show heavily corroded crystal edges (Fig. 6D). In TL, thermal microcracking is also prevalent in the lime crystal grains, while the periclase shows a "sponge-like" texture, significantly increasing intragranular microporosity (compare the insets in Figs. 6A

ACCEPTED MANUSCRIPT

and 6B). Texturally, the dolomite appears to be more severely affected by high temperatures than calcite, perhaps due to its lower decarbonation temperature (Fig. 3B).

3.2 Results of physical property analyses

3.2.1 "As-collected" physical properties

Plots of stress, cumulative AE energy, and *b*-value against strain for each of the room temperature UCS tests are presented in Figs. 7A and 7D. We also show the frequency-amplitude plots (for the entire experiment, Figs. 7B and 7E) and zoomed-in plots showing the *b*-value evolution at failure in more detail (Figs. 7C and 7F). The two rocks displayed a very different behaviour in response to the applied stress. Firstly, TL (peak stress of 112 MPa) was much stronger than MCL (peak stress of 29 MPa). TL was very brittle in the sense that it only showed a small degree of strain-hardening behaviour and, therefore, failure was characterised by a large stress drop, a substantial output of AE energy, and very low *b*-values. Meanwhile, MCL displayed a large degree of post-peak strain-softening or "roll-over" and, consequently, failure was slow and sluggish, characterised by much less AE energy and higher *b*-values than for TL. However, both samples failed by axial splitting (Figs. 7A and 7D), although the failure of TL was much more explosive. In both cases, macroscopic sample failure occurred at the peak in the output of AE and at the *b*-value minima (immediately following failure there was a small recovery in *b*-value). Our frequency-amplitude plots (Figs. 7B and 7E) show that deformation in TL was mainly accommodated by few, but high amplitude events (hence the low *b*-value, Fig. 7F), and that MCL was mainly accommodated by many low amplitude events (hence the high *b*-

ACCEPTED MANUSCRIPT

value, Fig. 7C). We note that the interpretation of our AE's and frequency-amplitude plots is conducted purely to explain the deformation style of our samples and, although they represent an analogy to seismicity, direct comparisons are ill-advised.

"As-collected" dry and wet ultrasonic wave velocities, dry and wet dynamic Young's modulus and Poisson's ratio, dry and wet Vp/Vs ratios, and dry static Young's modulus are given in Table 2. The data show that (1) both P- and S-wave velocities are higher in TL than MCL; (2) both static and dynamic Young's modulus are higher in TL than MCL; (3) the wet and dry Vp/Vs ratio and Poisson's ratio are very similar for both rocks; (4) wet velocities are only very slightly higher than dry velocities in both rocks; (5) wet dynamic Young's modulus is higher than the dry dynamic Young's modulus in both rocks; and (6) dynamic Young's modulus is higher than the static Young's modulus in both rocks.

3.2.2 Deformation at high *in-situ* temperatures

The stress-strain curves for the UCS tests at high *in-situ* temperatures of 500, 600, 650, and 800 °C are presented in Fig. 8A (for MCL) and Fig. 8C (for TL), together with the room temperature measurements of Fig. 7. The data show that the deformation behaviour of the two rocks changed from brittle (i.e., the ability of the rock to resist load decreases with permanent strain) at room temperature to ductile (i.e., the rock can accommodate permanent strain without losing the ability to resist load, see Rutter, 1986) at temperatures above 500 °C. For tests above 500 °C, deformation was arrested at 5% axial strain, during which time the samples did not fail (e.g., by axial splitting, see Fig. 7) but were "flowing" in response to the applied constant strain rate.

ACCEPTED MANUSCRIPT

The data show that, in both cases, strength was greatly reduced at temperatures exceeding 500 °C. The strength of TL suffered a greater reduction than MCL. For example, for TL, strength was reduced from 112 MPa at room temperature, to 75 MPa at 650 °C (a decrease of 33% from room temperature) and down to 23 MPa at 800 °C (a decrease of 79% from room temperature). For MCL, strength was reduced from 29 MPa at room temperature, to 19 MPa at 650 °C (a decrease of 34% from room temperature) and down to 14 MPa at 800 °C (a decrease of 52% from room temperature). The cumulative AE energy output for each of the high-temperature tests is given in Fig. 8B (for MCL) and Fig. 8D (for TL). The data show that AE energy output during deformation at temperatures higher than 500 °C was greatly reduced. At the end of the experiments, the stress was slowly reduced to zero, and the sample was cooled back to room temperature. To confirm that decarbonation had taken place in our experimental samples, we measured the mass of each and plotted the data (as open circles) on Fig. 3 (only for 600, 650, and 800 °C, since the sample at 500 °C failed by axial splitting). The data are in excellent agreement with our TG data (Fig. 3).

ACCEPTED MANUSCRIPT

3.2.3 Room temperature UCS experiments on thermally-stressed samples

The stress-strain curves for the UCS experiments performed at room temperature on samples thermally-stressed to 100, 200, 400, 500, 600, 650, and 700 °C (note: samples from thermal-stressing temperatures of 700 and 800 °C for MCL, and from the thermal-stressing temperature of 800 °C of TL, could not be tested due to their disintegration at high temperature; a result of portlandite formation, see explanation above) are presented in Fig. 9A (for MCL) and Fig. 9C

ACCEPTED MANUSCRIPT

(for TL), together with the experiments at room temperature from Fig. 7. The data shows that there was no systematic variation of strength with thermal-stressing temperature for TL (up to 700 °C, above 700 °C the sample disintegrated; Fig. 9C). Although, the four highest temperatures (500, 600, 650, and 700 °C) all failed at higher strains (about 0.9% strain compared to 0.6% for the temperatures below 500 °C). The MCL showed a similar trend: the experiments for the samples thermally-stressed to 500, 600, and 650 °C failed at 0.6% strain; below 500 °C the samples all failed at about 0.3% strain. However, for MCL, the three highest temperatures (500, 600, and 650 °C) also showed a reduction in strength when compared to the experiments below 500 °C. Below 500 °C the strength varied between 27 and 34 MPa. The strength was reduced to 22 MPa at both 500 and 600 °C, and to 18 MPa at 650 °C. All of the experiments, for both rock types, showed brittle behaviour and the samples failed by axial splitting. The output of AE for each of the experiments is given in Fig. 9B (for MCL) and Fig. 9D (for TL). In general, the output of AE was modest until macroscopic sample failure. The output of AE was not reduced at high thermal-stressing temperatures as they were for high *in-situ* temperatures (Fig. 8).

3.2.4 Physical property changes during thermal stressing

Exposure to high temperatures also resulted in severe changes to the physical properties of the carbonates (Fig. 10). Fig. 10A and Fig. 10B shows that their porosities increased slightly up to 500 °C, and then strongly up to the maximum temperature of 800 °C. Over the entire temperature range, the total porosity of TL increased by 19 percentage points and MCL increased by 13 percentage points (Fig. 10B). Fig. 10C shows that the bulk sample density

ACCEPTED MANUSCRIPT

remained constant up to about 500 °C (about 2.2 and 2.0 g.cm^{-3} for TL and MCL, respectively). Above 500 °C the density dropped rapidly and at 800 °C the bulk sample density was 1.4 and 1.1 g.cm^{-3} for TL and MCL, respectively.

The measured ultrasonic wave velocities for both dry and wet TL and MCL with increasing thermal-stressing temperature, together with the evolving Vp/Vs ratio, are given in Figs. 10D-H. For both TL and MCL, dry P- and S- wave velocities only demonstrated minor change up to 400 °C, but then decreased significantly up to the maximum temperature of 800 °C. Over the entire temperature range, dry P-wave velocities decreased by 54% and 67% and dry S-wave velocities by 44% and 60% for TL and MCL, respectively. The *in-situ* P-wave velocities display a similar trend (Fig. 10E), although the thermally-stressed values for MCL were slightly lower than the *in-situ* values. The dry Vp/Vs ratio remained roughly the same (about 1.7) until 700 °C when it decreased to about 1.6; it further decreased to about 1.5 at 800 °C (Fig. 10F). The wet ultrasonic measurements (note that the wet measurements could only be made for samples thermally-stressed up to 600 °C, beyond this temperature the water saturation method damaged the samples) were approximately the same as the dry measurements up to about 400 °C. Above 400 °C they started to decrease, but the rate of decrease was less than for the dry measurements. The wet Vp/Vs ratio remained at about 1.8 until 400 °C; above 400 °C it began to increase.

For both TL and MCL, dry dynamic Young's modulus and Poisson's ratio decreased as a function of thermal-stressing temperature (Fig. 10J). Dry dynamic Young's modulus decreased from 33.7 to 5.5 GPa (total decrease of 84%) and from 25.1 to 2.0 GPa (decrease of 92%) for a temperature increase from room temperature to 800 °C in TL and MCL, respectively (Fig. 10J).

ACCEPTED MANUSCRIPT

Within the same temperature interval, the dry dynamic Poisson's ratio decreased from 0.26 to 0.06 (total decrease of 76%) and from 0.27 to 0.13 (decrease of 51%) for TL and MCL, respectively. As to be expected, the evolution of dynamic elastic moduli with thermal-stressing temperature mirrored those for the ultrasonic wave velocities: the rate of change was low up to 400 °C, and then accelerated up to 800 °C. However, while the evolution of Young's modulus with thermal-stressing temperature for the wet measurements was similar to the dry measurements, the wet Poisson's ratio did not change significantly with increasing thermal-stressing temperature (Fig. 10I).

The evolution of the static Young's modulus with increasing thermal-stressing temperature, as calculated from the elastic portion of the stress-strain curves (see section 3.2.3), is presented in Fig. 10K. Firstly, we note that the static Young's modulus was lower than the dynamic Young's modulus (see Fig. 10J). Dynamic and static moduli generally differ due to their large differences in frequency (e.g., Simmons and Brace, 1965; Cheng and Johnston, 1981; Eissa and Kazi, 1989; Ciccotti *et al.*, 2000; Ciccotti and Mulargia, 2004). In the case of MCL, the evolution of the static Young's modulus with increasing TST was very similar to that of the dynamic values (little change up to 400 °C, followed by more significant changes). Although the evolution of static Young's modulus in TL was more clouded, there was still an overall decreasing trend. Over the entire temperature range, the static Young's modulus decreased by 42% and 76% for TL and MCL, respectively. We note that the data of Fig. 8k show only one value of Young's modulus in a material where it will be developing in an anisotropic manner, whereas thermal cracking usually produces an isotropically distributed crack network (e.g., David *et al.*, 1999).

ACCEPTED MANUSCRIPT

4. Discussion

Our study has illustrated that the chemical, mineralogical, and physical properties of two carbonates, chosen to span the heterogeneity seen within the Hyblean Plateau under Mt. Etna volcano, drastically changed upon exposure to high temperatures. We will now discuss our results in terms of (1) the hypothesised décollement at Mt. Etna volcano, (2) provide implications for the use of seismic wave velocities and elastic moduli during volcano monitoring, (3) present our CO_2 budget for the decarbonation of the carbonate basement and, (4) explore the importance of dolomite content within sub-volcanic carbonate successions.

4.1 Implications for décollements and flank instability at Mt. Etna

Flank deformation is often caused by slip along a décollement within or underneath a volcanic edifice. Although it has never been explicitly proven, décollement sliding surfaces have been inferred by many authors to exist under the eastern flank of Mt. Etna volcano, and have been blamed for large-scale gravity-driven deformation. To emphasise, geodetic data collected from the Pernicana Fault show that the eastern flank of the volcano is sliding towards the Ionion Sea at an average rate of about 2.8 cm/year (between April 1997 and February 1999, see Azzaro *et al.*, 2001; Palano *et al.*, 2008; Palano *et al.*, 2009). Active spreading and sliding at Mt. Etna volcano, monitored by interferometric synthetic aperture radar (INSAR), has provided evidence for a deep décollement zone at about 5 km depth (approximately at the intersection between the sediments of the Maghrebian-Appennine Chain and the Hyblean Plateau) in the form of an anticlinal ridge, believed to be the surface expression of a deep décollement (Borgia *et al.*, 2000; Froger *et al.*,

ACCEPTED MANUSCRIPT

2001; Lundgren *et al.*, 2004). This theory has been supported by field evidence (Borgia *et al.*, 1992; Tibaldi and Groppelli, 2002). Additional evidence was provided by the clustering of seismic activity below the eastern flank, at a depth of about 4 km (Acocella *et al.*, 2003; Neri *et al.*, 2004). It must be noted that some authors have suggested that movement occurs along another décollement, located at a depth of between 1.5 and 3 km (Bonforte and Puglisi, 2003; Palano *et al.*, 2008).

Our experimental data has shown that rock chosen to represent the deep Hyblean Plateau becomes considerably weaker at high *in-situ* temperatures (for instance, at 800 °C a strength reduction of 79% and 52% was observed for TL and MCL, respectively), and does not fail by shear faulting or axial splitting, but "flows" in a ductile manner (i.e., without localisation). We speculate that the observed thermally-induced weakening and distributed ductile deformation are the result of intracrystalline plasticity (see detailed studies on calcitic rocks by Rutter, 1974; Schmidt *et al.*, 1980), although it is difficult to interpret the interplay between decarbonation [which still progressed (see the open circles on Fig. 3), meaning that MCL was composed entirely of lime and TL of lime and periclase] and intracrystalline plasticity without further, more detailed analyses. Lime and periclase are weaker than calcite and dolomite; for instance, periclase layers acted as high-strain shear zones in torsion experiments on dolomite marble (Delle Piane *et al.*, 2007).

The ductile deformation of the carbonates of the Hyblean Plateau could explain the large-scale deformation and flank movement measured at Mt. Etna volcano (e.g., reported in Azzaro *et al.*, 2001; Palano *et al.*, 2008; Palano *et al.*, 2009), rather than slip on an inferred localised

ACCEPTED MANUSCRIPT

décollement surface (Fig. 1). Recent edifice-stability modelling has demonstrated that large-edifice collapse and the generation of catastrophic debris avalanches at stratovolcanoes can be attributed to the magma supply rate, but only if the basement conditions are stable over long periods (Zernack *et al.*, 2012). While this may be appropriate for numerous volcanoes, including their case study (Mount Taranaki, New Zealand) where the Tertiary basement rocks are inferred to be stronger than the overlying volcanics, it may not be true for volcanoes with a dynamic and unstable carbonate basement. Mt. Etna could also be at risk to large-scale deformation due to the preferential weakening of the Hyblean Plateau with respect to the sediments of the Maghrebian-Appennine Chain. This is a product of the fact that (1) the rocks of the Maghrebian-Appennine Chain will suffer, on the whole, less by the way of thermal weakening; for instance, quartz-arenitic rocks will not undergo decarbonation and intracrystalline plasticity in calcite can be achieved at relatively moderate temperatures and pressures [largely attributed to the low shear stresses required to initiate mechanical twinning and dislocation slip in calcite (Turner *et al.*, 1954; Griggs *et al.*, 1960)] and, (2) the important heat sources are located within the Hyblean Plateau. Thus preferential weakening will generate a greater rheological contrast between the two layers. Previously, it has been demonstrated experimentally that spreading induced by volcanic loading is strongly dependent on whether (1) there is a weak layer in the substratum, that is (2) overlain by a relatively thin brittle layer (Merle and Borgia, 1996). This is indeed the scenario at Mt. Etna volcano. Complimentary experiments have also highlighted that the distribution and alteration of a weak substratum can become a major factor in shaping volcano architecture (Walter and Troll, 2003). A similar process is thought to be occurring at Mt. Vesuvius, where sliding is thought to be taking place at the contact of the volcanic material and the underlying carbonatic basement, driving gravitational sliding and subsidence (Lanari *et al.*,

ACCEPTED MANUSCRIPT

2002). Our data also show that, at temperatures above 500 °C, the ductile deformation of the carbonates proceeds with a significantly reduced output of AE's (a proxy for seismicity). This switch from microcracking to intracrystalline plasticity (only inferred in our case) could be the reason for the discrepancy between (1) the shallow and very energetic seismic swarms associated with flank slip and the more limited seismic activity in the deep basement (Allard *et al.*, 2006) and, (2) the seismicity expected from the numerical modelling of dyke stresses and observed seismicity data (e.g., Roman and Cashman, 2006).

The authors are certainly aware that the rocks of the Hyblean Plateau are situated at a depth of 5 km (equating to confining pressures of about 70-80 MPa), and although we have performed uniaxial experiments at ambient pressure, we contend that (1) the reductions in strength are commensurate with those seen solely as a result of increasing temperature (or at least a first-order approximation) under triaxial conditions and, (2) an increase in pressure will only act to reduce the temperature required for ductility and "flow". Let us first consider the effect of confining pressure on the reductions of strength seen in limestone at elevated temperatures. As an example, Solnhofen limestone (99.9 wt.% calcite) has been shown to weaken with temperature under triaxial stress conditions (Xiao *et al.*, 2003). Under an effective pressure of 50 MPa, the strength was reduced from 360 MPa at room temperature, to 351 MPa at 50 °C (reduction of 2.5% when compared to room temperature), 330 MPa at 100 °C (reduction of 6%), and 306 MPa at 200 °C (reduction of 7.3%). These reductions in triaxial strength, if extrapolated to higher temperatures, are certainly in agreement with our uniaxial strength reductions (although the absolute values will, of course, be different). Let us now consider the effect of confining pressure on the brittle-ductile transition. Although our uniaxial data suggest that ductile

ACCEPTED MANUSCRIPT

behaviour is achieved at temperatures greater than 500 °C (Fig. 8) it is likely that, due to the contributing influence of the high effective pressures at 5 km (about 70-80 MPa), ductility would be achieved at much lower temperatures. In the case of low porosity carbonates, ductility can be achieved at room temperature at effective pressures above 100 MPa (Baud *et al.*, 2000). For higher porosity carbonates (like the ones of our study), the transition will occur at lower pressures (Evans *et al.*, 1990). It is therefore possible that much of the Hyblean Plateau could deform in a ductile manner in response to stress, even far from the heat sources. High temperature triaxial experiments are now needed to map out the brittle-ductile transition under the relevant pressure and temperature conditions. Further, there are a couple of extra ideas to consider. First, high porosity limestones are also prone to inelastic compaction (grain crushing and pore collapse), termed P*, at elevated pressures (Baud *et al.*, 2009). Baud *et al*. (2009) showed that, for Majella limestone (30% porosity) and Saint-Maximin limestone (37% porosity), P* was about 26.5 MPa and 13 MPa (both pressures represent depths above that of the Hyblean Plateau) for wet conditions, respectively. Second, our experiments were performed under dry conditions (rock at depth is likely to contain a fluid phase); it has been previously shown that the presence of water can also influence the strength and ductility through physico-chemical processes at grain boundaries and via the law of effective stress (Rutter, 1972).

4.2 Implications on the use of seismic velocities in monitoring at Mt. Etna

A dense seismic network, run by Istituto Nazionale di Geofisica e Vulcanologia, Sezione di Catania (INGV-CT), is constantly monitoring seismic events at Mt. Etna volcano. Tomographic inversions of P- and S-wave arrival times of volcano-tectonic earthquakes have been computed

ACCEPTED MANUSCRIPT

using a variety of techniques (see Chiarabba *et al.*, 2004 for a review). Low ultrasonic wave velocity zones (or a high Vp/Vs ratio) are commonly interpreted as fractured or damaged zones (a higher Vp/Vs ratio suggests that there is a higher crack density in saturated rock, see O'Connell and Budiansky, 1974) or are interpreted as the result of the presence of fluids (e.g., Zhang *et al.*, 2009), while high ultrasonic wave velocity zones (or a low Vp/Vs ratio) are commonly interpreted as intrusions or magma bodies (e.g., see Laigle *et al.*, 2000; Patanè *et al.*, 2002; Aloisi *et al.*, 2002; Patanè *et al.*, 2006). This technique has therefore been used to monitor magma movement preceding volcanic eruptions (e.g., Patanè *et al.*, 2006).

Our experimental data demonstrate that ultrasonic wave velocities decreased with increasing temperature for both carbonates. Over the entire temperature range (from room temperature to 800 °C), dry P-wave velocities decreased by 54% and 67% and dry S-wave velocities by 44% and 60% for TL and MCL, respectively. The wet measurements did not differ greatly from the dry measurements, although the rate of the velocity decrease above 400 °C was reduced. Ultrasonic wave velocities are very sensitive to microcracks (see O'Connell and Budiansky, 1974; Toksöz *et al.*, 1976), therefore the difference between dry and wet P-waves velocity measurements is usually large for pervasively microcracked materials (since P-waves travel faster through water than air). However, in the case of limestones, due to the nature of their formation, the porosity is made up of mostly pores and consequently dry and wet velocities are generally very similar. The fact that the rate of velocity decrease was retarded upon water saturation in our measurements suggests that the observed decrease was the result of thermal microcracking (see Toksöz *et al.*, 1976); indeed, we see many more microcracks in the thermally-stressed samples (see Fig. 6). Thermal microcracking has been previously observed to

ACCEPTED MANUSCRIPT

occur in carbonates at similar temperatures (Homand-Etienne and Troalen, 1984; Fredrich and Wong, 1986). The changes observed for the limestones investigated in this study were greater than those observed for the marly limestone studied by Mollo *et al*. (2011a). Over roughly the same temperature range, the P-wave velocity of the two limestones containing a very high total (> 95 wt.%) carbonate content (TL and MCL) decreased by twice that of the marly limestone (comprising only 75 wt.% calcite), found within the melange of marly clays, marly limestones and quartz-arenitic rocks that overly the Hyblean Plateau. This is likely to be due to the fact that, since decarbonation plays such a key role in the demise of the ultrasonic wave velocities, the more carbonate present in the rock, the greater their capacity for reduction. Our dry Vp/Vs ratio data show that initially the Vp/Vs ratio was about 1.7, but was reduced to about 1.6 at 700 °C, and then further to 1.5 at 800 °C. The wet Vp/Vs ratio remained at about 1.8 until 400 °C; above 400 °C it began to increase. A decrease in the dry Vp/Vs ratio and an increase in the wet Vp/Vs ratio with increasing crack damage has been observed previously (Nur and Simmons, 1969; O'Connell and Budiansky, 1974; Wang *et al.*, 2012).

The well-known anomalously low P-wave velocity zone at Mt. Etna (see Aloisi *et al.*, 2002) has been estimated at a depth between 3-4 km, and is therefore located on the cusp of the Hyblean Plateau, within the melange of marly clays, marly limestones, and quartz-arenitic rocks. Devolitisation reactions have been recently proposed as a potential cause of the low velocity zones present in the Maghrebian-Appennine Chain (Mollo *et al.*, 2011a). Although smaller low velocity zones are located at depths corresponding to the Hyblean Plateau (Aloisi *et al.*, 2002), it is likely that, in general, due to their deeper location, the carbonates of the Hyblean Plateau have

ACCEPTED MANUSCRIPT

undergone some degree of pore collapse after their initital decarbonation, resulting in a re-increase of their elastic wave velocities.

Perhaps the Vp/Vs ratio holds the greatest potential for volcanic subsurface interpretation. Our data suggest that the extensive microcracking and porosity increase associated with decarbonation serve to increase the Vp/Vs ratio, assuming that the rock is saturated. We suggest that the anomalously high Vp/Vs ratios seen by Aloisi *et al*. (2002) and Patanè *et al*. (2006) could be explained by the rapid migration of magmatic gas/fluids from an intruion zone into recently calcinated, intensely fractured carbonate rocks. However, we note that in a scenario where dry, fractured zones could be expected, the Vp/Vs interpretation of the subsurface should be handled with extreme care. Further, a recent study by Wang *et al*. (2012) suggested that crack anisotropy should also be considered in Vp/Vs analyses.

4.3 Implications on the use of elastic moduli in volcano monitoring at Mt. Etna

Our experimental data showed that dynamic and static Young's modulus, and dry dynamic Poisson's ratio decreased, whilst wet dynamic Poisson's ratio increased with increasing thermal-stressing temperature for both carbonates. The knowledge of elastic moduli, and by how much they can change in response to thermal and mechanical stresses, is important for many facets of volcano monitoring and stability studies, such as (1) ground deformation modelling (e.g., see Manconi *et al.*, 2007; Manconi *et al.*, 2010), (2) the calibration of damage mechanics criteria (Voight, 1989; Kilburn, 2003; Kilburn and Sammonds, 2005), (3) the application of simple failure criteria (such as that of Hoek and Brown, 1997; e.g., Apuani *et al.*, 2005), (4) the

ACCEPTED MANUSCRIPT

understanding of dyke propagation and arrest (Gudmundsson, 2009; Gudmundsson, 2011), (5) the determination of accurate universal-scaling laws for fault displacement (Gudmundsson, 2004) and, (6) the determination of stress rotation (Faulkner *et al.*, 2006; Heap *et al.*, 2010).

Previous experimental work (e.g., Heap *et al*. 2010) designed to help constrain these physical properties, reported the evolution of static elastic moduli with increasing stress-induced cyclic uniaxial damage for three rock types (granite, basalt, and sandstone). In general, for all three rock types, static Young's modulus decreased by 10-30% and Poisson's ratio increased by up to a couple of hundred per cent (Heap *et al.*, 2010; see also Eberhardt *et al.*, 1999; Lau and Chandler, 2004). Mechanical stresses have also been shown to reduce dynamic Young's modulus by a similar percentage (e.g., Ayling *et al.*, 1995). Changes in dynamic (Alm *et al.*, 1985; Petrakova *et al.*, 2012) and static (Heard and Page, 1982; Homand-Etienne and Houpert, 1989; Heap *et al.*, 2009; Petrakova *et al.*, 2012) elastic moduli in response to thermal stressing showed that, whereas granites showed a deterioration in elastic moduli (e.g., Young's modulus was decreased by between 50-70%), extrusive igneous rocks (basalt and andesite) were unaffected. In the case of the extrusive igneous rocks, the unaltered elastic moduli were interpreted to be a consequence of their pre-existing pervasive thermal microcrack network (perhaps linked to the notion of the Kaiser "temperature memory" effect, see Yong and Wang, 1980; Zuberek *et al.*, 1999; Choi *et al.*, 2005) and their thermally stable mineral assemblages (Heap *et al.*, 2009; Petrakova *et al.*, 2012).

Our data show that the Young's modulus of two carbonates decreased more in response to thermal-stressing (the dynamic Young's modulus in this study decreased by 84% and 92% and

ACCEPTED MANUSCRIPT

the static Young's modulus by 42% and 76% over the entire temperature range (room temperature to 800 °C for TL and MCL, respectively) than a variety of other crustal rocks (granite, basalt, sandstone, and andesite) in response to either thermal or mechanical stressing. Over the same range in temperature, the dry dynamic Poisson's ratio decreased by 76% and 51% for TL and MCL, respectively. Whereas the Poisson's ratio of rock is expected to decrease with increasing crack density (see O'Connell and Budiansky, 1974), recent uniaxial cyclic-stressing experiments have shown it to increase dramatically with increasing damage (Heap *et al.*, 2010). This discrepancy is likely the result of preferential axial microcrack development during uniaxial compression; samples thermally-stressed under ambient pressure conditions have been shown to develop an isotropic microcrack network (e.g., Menéndez *et al.*, 1999; David *et al.*, 1999).

We can conclude that (1) mineralogical changes (and in particular decarbonation) and phase transitions give raise to the most significant changes in the elastic moduli of rocks: e.g., decarbonation (in the case of carbonates, this study), the α-β quartz transition (in granites and sandstones, see Glover *et al.*, 1995), and the loss of water from zeolites (in pyroclastic deposits, see Heap *et al.*, 2012). In the absence of chemical alteration, and when the rocks already contain an extensive thermal microcrack network [the case for the basalt of Heap *et al*. (2009) and the andesite of Petrakova *et al*., 2012], no changes were observed. (2) Care must be taken when, for example, selecting elastic parameters to model ground deformation and, where necessary, multi-layer elastic half-space models such be utilised (Manconi *et al.*, 2010). Moreover, dynamic and static moduli generally differ due to their large differences in frequency (e.g., Simmons and Brace, 1965; Cheng and Johnston, 1981; Eissa and Kazi, 1989; Ciccotti *et al.*, 2000; Ciccotti and Mulargia, 2004). Recently, Manconi *et al*. (2010) suggested that static elastic moduli are more

ACCEPTED MANUSCRIPT

appropriate in finite-element ground deformation modelling than dynamic elastic moduli. (3) While the reduction in strength due to decarbonation may allow dykes to propagate within the carbonates of the Hyblean Plateau more easily (dyke-induced mechanical and thermally generated pore fluid pressures can severely affect flank stability, see Elsworth and Voight, 1996), the increase in the elastic mismatch between these decarbonated sediments and the layers above could also facilitate dyke arrest (Gudmundsson, 2011).

4.4 The CO_2 paradox at Mt. Etna

It is well known that CO_2 is exsolved and released by ascending magma, due to its abundance and low solubility in silicate melts (Stolper and Holloway, 1988; Pan *et al.*, 1991; Papale, 1999). For this reason, CO_2 degassing has been used as an indicator of the pre-eruptive ascent of magma (e.g., Giammanco *et al.*, 1998; Bruno *et al.*, 2001; Gerlach *et al.*, 2002; Aiuppa *et al.*, 2006) and as a proxy for the magma volume present. However, at Mt. Etna volcano, these estimates usually grossly overestimate the volume of magma (e.g., see D'Alessandro *et al.*, 1997). D'Alessandro *et al*. (1997) report that calculations over the period 1971-1995 resulted in a volume of magma approximately twenty times greater than the erupted volume. In the case of Mt. Etna it appears clear that a significant contribution must come from a "non-magmatic source". This discrepancy has been postulated to be due to an anomalously shallow asthenosphere that permits the continuous escape of CO_2 (D'Alessandro *et al.*, 1997) or from the decarbonation of the sedimentary substratum at Mt. Etna (e.g. see Allard *et al.*, 1991; Frezzotti *et al.*, 2009; Chiodini *et al.*, 2011). In these scenarios, the contribution of decarbonation to the CO_2 budget at Mt. Etna volcano remains overlooked. We are now in a position, using our new experimentally-obtained

ACCEPTED MANUSCRIPT

decarbonation onset temperatures (Fig. 3) and recent thermo-mechanical numerical modelling data (Del Negro *et al.*, 2009; Bonaccorso *et al.*, 2010), to provide the first estimate for Mt. Etna volcano.

The volume of the affected aureole (V) can be calculated via the length of the inner and outer, long and short axes (a_i, a_o, b_i, b_o, respectively), using the ellipsoidal (as per the calculations of Bonaccorso *et al.*, 2010) relationship:

$$V = 4/3\ \pi\ (a_o\text{-}a_i)^2(b_o\text{-}b_i) \qquad (7)$$

The volume estimate using a reaction initiation temperature of 560°C for TL (Fig. 1b), corresponds to an aureole with the dimensions a_i = 1.2 km, a_o = 2.7 km, b_i = 3.1 km, and b_o = 4.0 km, and yields a volume of 8.5 km^3. In contrast, in our computation of an aureole using a reaction initiation temperature of 680°C for MCL, we obtain dimensions of a_i = 1.2 km, a_o = 2.0 km, b_i = 3.1 km, and b_o = 3.4 km and estimate that approximately 3.5 km^3 of carbonate is at risk to decarbonation. Using densities of 2.21 and 2.01 Mt/km^3 for TL and MCL (Table 2), respectively, we estimate their respective masses in the aureole to be 18.8 and 7.0 Mt. In our chemical analysis, we note that each limestone yields approximately 44 wt.% of CO_2 upon complete decarbonation (Fig. 5 and Table 1). Thus, we estimate that decarbonation of the carbonates would have liberated as much as 8.3 and 3.1 Mt of CO_2, respectively – a substantial amount of CO_2. Between 1977-1984 the summit plume at Mt. Etna volcano was releasing about 35 kt of CO_2 per day (Allard *et al.*, 1991), resulting in a yearly output of about 13 Mt. More

ACCEPTED MANUSCRIPT

recent measurements (2004-2005) have yielded lower emanation rates of about 9 kt per day or 3.3 Mt per year (Aiuppa *et al.*, 2006).

Although this highlights that sub-volcanic decarbonation should not be dismissed when considering the CO_2 budget at Mt. Etna, it could be argued that the carbonate surrounding the long-lived magmatic body used in the calculation has long since decarbonated. However, as explained above, magmatic activity at Mt. Etna is constantly evolving and recent flank eruptions were sourced from new reservoirs and new pathways emplaced within the carbonatic basement (Behncke and Neri, 2003; Acocella and Neri, 2003; Andronico *et al.*, 2005; Carbone *et al.*, 2009; Bonforte *et al.*, 2009); therefore new volumes of carbonate rock may well be readily available for decarbonation.

4.5 An important role for dolomite within a sub-volcanic sedimentary substratum?

In general, the physical properties of TL suffered more than MCL when exposed to magmatic temperatures. This may be explained by a lower initial porosity, resulting in a greater relative deterioration (despite the fact that mass loss from decarbonation was almost identical). This raises the question of the importance of dolomite content within the sedimentary basements of active volcanoes. We have seen that dolomite (1) dissociates at lower temperatures than calcite and (Fig. 3), (2) is more readily altered than calcite after exposure to 800 °C (Fig. 6). Previously, an increase in dolomite content has been shown to have a strengthening influence on carbonate rock at room temperature (see Kennedy and Cleven, 2011). The room temperature data of this study corroborate with this hypothesis; our study has shown TL to be much stronger than MCL

ACCEPTED MANUSCRIPT

(TL had a UCS of 112 MPa, compared to 29 MPa for MCL, see Fig. 7). Although, the difference in UCS is likely to reflect the significant difference in porosity (TL = 18.4%, and MCL = 25.2%) and/or grain size (TL = 10-25 μm, and MCL = 100-400 μm). Here, combining these observations, we can conclude that, whereas the presence of dolomite at low temperatures may act to strengthen the substratum, it will make it more prone to weakening during decarbonation at high temperatures. A similar conclusion was drawn from large strain torsion experiments on calcite-dolomite composite rocks (Delle Piane *et al.*, 2008).

5. Conclusions

1. We have shown, for two different carbonates, chosen to represent the vast heterogeneity seen within the Hyblean Plateau under Mt. Etna volcano, that high temperatures will strongly influence their chemical, physical, and mechanical properties, particularly after decarbonation.
2. A major mass loss, associated with decarbonation, took place in the temperature range of 680-882 °C and 560-905 °C for MCL and TL, respectively. In total, for both carbonates, their mass decreased by about 45 wt.% and they released about 44 wt.% of CO_2. XRPD analysis confirmed the loss of calcite and dolomite at high temperatures.
3. These debilitating chemical changes had a dramatic influence on the physical properties of the two investigated carbonates. Porosity, wet dynamic Poisson's ratio, and wet Vp/Vs ratio all increased, whilst P- and S-wave velocities, bulk sample density, dynamic and static Young's modulus, dry Vp/Vs ratio, and dry dynamic Poisson's ratio all decreased.

ACCEPTED MANUSCRIPT

4. The strength of the carbonates was dramatically reduced at high *in-situ* temperatures. At and above 500 °C, the samples did not fail, but "flowed" aseismically in a ductile manner. We suggest that thermally-induced weakening of the Hyblean Plateau could therefore encourage the large-scale deformation measured at Mt. Etna volcano.
5. We suggest that the changes in physical properties observed after exposure to high temperatures can help explain (1) low seismic velocity zones present within the sub-volcanic basement at Mt. Etna, (2) the anomalously high Vp/Vs ratios and the rapid migration of fluids, both observed at Mt. Etna and, (3) the increasing instability of volcanic edifices in the lifespan of a magmatic system.
6. The data also suggest that care must be taken when selecting elastic parameters (1) to model ground deformation in active geothermal and volcanic regions, (2) for the calibration of damage mechanics criteria and, (3) when applying simple failure criteria to studies of volcano flank stability.
7. We also provide the first CO_2 budget for the decarbonation of the sedimentary substratum at Mt. Etna, using recent thermo-mechanical numerical models and our experimental data. We estimate that decarbonation could have liberated as much as 8.3 Mt of CO_2. We highlight that sub-volcanic decarbonation should not be dismissed when considering the CO_2 budget at Mt. Etna.

Acknowledgements

The authors would like to thank P. Tuccimei and S. Soligo for the use of their analytical facilities at the Dipartimento di Scienze Geologiche of the University "Roma Tre" in Rome, and Thierry

ACCEPTED MANUSCRIPT

Reuschlé for his help at the Université de Strasbourg. The paper has also benefitted from discussions with Alex Kushnir. M. Heap was funded by the German Federation of Materials Science and Engineering (BV MatWerk) and the German Research Foundation (DFG). Y. Lavallée acknowledges support from the DFG grant LA2651/1-1. This work was also supported by ERC Starting Grants GLASS (#259256) and SLiM (#306488), and ERC Advanced Grant EVOKES (#247076). D. B. Dingwell also acknowledges support of a research professorship of the Bundesexzellenzinitiative (LMUexcellent). M. J. Heap and D. B. Dingwell acknowledge the support of a Hubert Curien Partnership (PHC) PROCOPE grant (grant number 27061UE), the Deutscher Akademischer Austauschdienst (DAAD) in Germany, and the Ministry of Foreign and European Affairs (MAE) and the Ministry of Higher Education and Research (MESR), both in France. We appreciated the constructive comments of Giuseppe Puglisi and three anonymous reviewers.

ACCEPTED MANUSCRIPT

ACCEPTED MANUSCRIPT

Table One

The "as-collected" chemical properties of TL and MCL determined by ICP-AES. The detection limit for the data is 0.01%. For the analyses, the powdered samples were mixed with a flux of lithium metaborate and lithium tetraborate, and then fused in an induction furnace at a temperature of 1100 °C.

	Thala limestone (TL) (wt.%)	**Mt. Climiti limestone (MCL) (wt.%)**
SiO_2	2.12	0.70
Al_2O_3	0.48	0.23
Fe_2O_3	0.18	0.18
MgO	3.56	0.44
CaO	49.88	54.49
Na_2O	0.04	0.04
K_2O	0.07	0.04
P_2O_5	0.05	0.05
Total	56.38	56.17

ACCEPTED MANUSCRIPT

ACCEPTED MANUSCRIPT

Table Two

The "as-collected" physical properties of TL and MCL. UCS and the ultrasonic wave velocities were both measured at room temperature. The connected porosities were measured using the triple weight water saturation technique.

	Thala limestone (TL)	**Mt. Climiti limestone (MCL)**
Connected porosity (%)	18.4	25.2
Bulk sample density (g.cm^{-3})	2.21	2.01
Calcite-dolomite ratio	78-22	100-0
Grain size (µm)	10-25	100-400
Dry UCS (MPa)	112	29
Dry P-wave velocity (km.s^{-1})	4.32	3.97
Wet P-wave velocity (km.s^{-1})	4.40	4.14
Dry S-wave velocity (km.s^{-1})	2.46	2.21
Wet S-wave velocity (km.s^{-1})	2.44	2.31
Dry Vp/Vs ratio	1.75	1.79
Wet Vp/Vs ratio	1.88	1.79
Dry dynamic Young's modulus (GPa)	33.74	25.12
Wet dynamic Young's modulus (GPa)	34.19	30.69
Dry dynamic Poisson's ratio	0.26	0.27
Wet dynamic Poisson's ratio	0.30	0.27
Static Young's modulus (GPa)	27.8	15.7

ACCEPTED MANUSCRIPT

Figure captions

Figure 1. Schematic of Mt. Etna volcano (redrawn from Tibaldi and Groppelli, 2002) highlighting the positions of the heat sources in relation to the Hyblean Plateau.

Figure 2. A: Schematic diagram of the uniaxial press at the Laboratoire de Déformation des Roches (IPGS, Strasbourg). B: Schematic diagram of the high temperature uniaxial press at Ludwig-Maximilians University (LMU, Munich).

Figure 3. Thermo-gravimetric (TG) and scanning differential calorimetry (DSC) curves for "as-collected" samples of (A) MCL and (B) TL. Part of the DSC curve in (D) has been blown up to better show the endothermic peaks at 775 and 810 °C. The open circles represent mass measurements of the 600, 650, and 800 °C post-deformation samples shown in Fig. 8 (see text for details).

Figure 4. X-ray powder diffraction patterns for TL and MCL at 25, 200, 400, 600, 650 and 800 °C. Cc, calcite; Dm, dolomite; Pt, portlandite; Li, lime; Pe, periclase. All of the graphs are plotted on the same scale. However, for the 800 °C plots, blown up versions are provided to better highlight the new peaks.

Figure 5. Carbonate loss and CO_2 release from TL and MCL measured at 25, 200, 400, 600, 650, and 800 °C measured by mass-loss-on-calcination and calcimetry analysis.

ACCEPTED MANUSCRIPT

Figure 6. FE-SEM compositional photomicrographs of samples of TL and MCL, on "as-collected" samples, (A) and (C), and samples thermally-stressed to 800 °C, (B) and (D). Cc, calcite; Dm, dolomite; Li, lime; Pe, periclase. Scale bars are 50 µm. Insets in (A) and (B) are designed to highlight the difference between the intact dolomite grains and the periclase grains after exposure to high temperatures. Inset in (D) highlights the thermal microcracking within the lime crystals of MCL.

Figure 7. Axial stress-strain curves, acoustic emission output, and *b*-values for MCL (A) and TL (B) from room temperature uniaxial experiments performed at a constant strain rate of 1.0×10^{-5} s^{-1}. *b*-values were calculated using Aki's maximum likelihood method (Aki, 1965) for every 200 AE hits at 100 hit intervals. The failed samples are shown as insets on each figure. Frequency-amplitude plots for the all of the AE's during the experiments are shown for MCL (B) and TL (E), and zoomed-in plots of the *b*-value evolution at failure are given in (C) and (F) for MCL and TL, respectively.

Figure 8. Axial stress-strain curves for MCL (A) and TL (C) at high *in-situ* temperatures of 500, 600, 650, and 800 °C, plotted together with the stress-strain curves for room temperature given in Fig. 5. Experiments were performed at a constant strain rate of 1.5×10^{-5} s^{-1}. The output of cumulative AE energy for the experiments are given in (B) and (D) for MCL and TL, respectively.

Figure 9. Axial stress-strain curves for thermally-stressed (the thermal-stressing temperature for each curve is given on the figure) MCL (A) and TL (C) at room temperature. Experiments were

ACCEPTED MANUSCRIPT

performed at a constant strain rate of 1.0 x 10^{-5} s^{-1}. The output of cumulative AE energy for the experiments are given in (B) and (D) for MCL and TL, respectively.

Figure 10. The degradation of MCL and TL rock physical properties with increasing thermal stressing temperature. (A) Connected porosity; (B) total porosity change; (C) bulk sample density; (D) dry ultrasonic wave velocities; (E) *in-situ* P-wave velocities; (F) dry Vp/Vs ratio; (G) wet ultrasonic wave velocities; (H) wet Vp/Vs ratio; (I) wet dynamic elastic moduli; (J) dry dynamic elastic moduli; (K) dry static elastic moduli;

ACCEPTED MANUSCRIPT

ACCEPTED MANUSCRIPT

References

Acocella, V., Behncke, B., Neri, M. and D'Amico, S., 2003. Link between major flank slip and 2002–2003 eruption at Mt. Etna (Italy), *Geophysical Research Letters*, **30**, No. 24, 2286, doi:10.1029/2003GL018642.

Acocella, V. and Neri, M., 2003. What makes flank eruptions? The 2001 Etna eruption and its possible triggering mechanisms *Bulletin of Volcanology*, **65**, 517-529.

Acocella, V. and Puglisi, G., 2012. How to cope with volcano flank dynamics? A conceptual model behind possible scenarios for Mt. Etna, *Journal of Volcanology and Geothermal Research*, doi:10.1016/j.jvolgeores.2012.06.016.

Ague, J. J., 2003. Fluid infiltration and transport of major, minor, and trace elements during regional metamorphism of carbonate rocks, Wepawaug Schist, Connecticut, USA, *American Journal of Science*, **303**, 753-816.

Aiuppa, A., Federico, C., G., G., Gurrieri, S., Liuzzo, M., Shinohara, H., R., F. and Valenza, M., 2006. Rates of carbon dioxide plume degassing from Mount Etna volcano, *Journal of Geophysical Research*, **111**, B09207, doi:10.1029/2006JB004307.

Aki, K., 1965. Maximum likelihood estimate of b in the formula log N=a-bM and its confidence limits, *Bull. Earthq. Res. Inst.*, **43**, 237-239.

Allard, P., Behncke, B., D'Amico, S., Neri, M. and Cambino, S., 2006. Mount Etna 1993–2005: Anatomy of an evolving eruptive cycle, *Earth Science Reviews*, **78**, 85-114.

Allard, P., Carbonnelle, J., Dajlevic, D., Le Bronec, J., Morel, P., Robe, M. C., Maurenas, J. M., Faivre-Pierret, R., Martin, D., Sabroux, J. C. and Zettwoog, P., 1991. Eruptive and diffuse emissions of CO_2 from Mount Etna, *Nature*, **351**, 387-391.

Alm, O., Jaktlund, L. and Shaoquan, K., 1985. The influence of microcrack density on the elastic and fracture mechanical properties of Stripa granite, *Physics of the Earth and Planetary Interiors*, **40**, 161-179.

Aloisi, M., Bonaccorso, A., Cannavo, F., Cambino, S., Mattia, M., Puglisi, G. and Boschi, E., 2009. A new dyke intrusion style for the Mount Etna May 2008 eruption modelled through continuous tilt and GPS data, *Terra Nova*, **21**, 316-321.

Aloisi, M., Cocina, O., Neri, M., Orecchio, B. and Privitera, E., 2002. Seismic tomography of the crust underneath the Etna volcano, Sicily, *Phys. Earth Planet. Inter.*, **134**, 139-155.

Alparone, S., Barberi, E., Cocina, O., Giampiccolo, E., Musumeci, C. and Patané, D., 2012. Intrusive mechanism of the 2008–2009 Mt. Etna eruption: Constraints by tomographic images and stress tensor analysis, *Journal of Volcanology and Geothermal Research*, **229-230**, 50-63.

Andronico, D., Branca, S., Calvari, S., Burton, M., Caltabiano, T., Corsaro, R. A., Del Carlo, P., Garfi, G., Lodato, L., Miraglia, L., Murè, F., Neri, M., Pecora, E., Pompilio, M., Salerno, G. and Spampinato, L., 2005. A multi-disciplinary study of the 2002–03 Etna eruption: insights into a complex plumbing system, *Bulletin of Volcanology*, **67**, 314-330.

ACCEPTED MANUSCRIPT

Apuani, T., Corazzato, C., Cancelli, A. and Tibaldi, A., 2005. Physical and mechanical properties of rock masses at Stromboli: a dataset for volcano instability evaluation, *Bull. Eng. Geol. Env.*, **64**, 419-431.

Ayling, M. R., Meredith, P. G. and Murrell, S. A. F., 1995. Microcracking during triaxial deformation of porous rocks monitored by changes in rock physical properties, I. Elastic-wave propagation measurements on dry rocks, *Tectonophysics*, **245**, 205-221.

Azzaro, R., Mattia, M. and Puglisi, G., 2001. Fault creep and kinematics of the eastern segment of the Pernicana Fault (Mt. Etna, Italy) derived from geodetic observations and their tectonic significance, *Tectonophysics*, **333**, 401-415.

Balashov, V. N. and Yardley, B. W. D., 1998. Modeling metamorphic fluid flow with reaction-compaction-permeability feedbacks, *American Journal of Science*, **298**, 441-470.

Balme, M. R., Rocchi, V., Jones, C., Sammonds, P. R., Meredith, P. G. and Boon, S., A., 2004. Fracture toughness measurements on igneous rocks using a high-pressure, high-temperature rock fracture mechanics cell, *Journal of Volcanology and Geothermal Research*, **132**, 159-172.

Barnes, C. G., Prestvik, T., Sundvoll, B. and Surratt, D., 2005. Pervasive assimilation of carbonate and silicate rocks in the Hortavær igneous complex, North-Central Norway, *Lithos*, **80**, 179-199.

Baud, P., Schubnel, A. and Wong, T.-F., 2000. Dilatancy, compaction, and failure mode in Solnhofen limestone, *Journal of Geophysical Research*, **105, No. B8**, 19289-19303.

Baud, P., Vinciguerra, S., David, C., Cavallo, A., Walker, E. and Reuschlé, T., 2009. Compaction and failure in high porosity carbonates: Mechanical data and microstructural observations, *Pure and Applied Geophysics*, **166**, 869-898.

Behncke, B. and Neri, M., 2003. The July–August 2001 eruption of Mt. Etna (Sicily), *Bulletin of Volcanology*, **65**, 461-476.

Benson, P. M., Thompson, A. B., Meredith, P. G., Vinciguerra, S. and Young, R. P., 2007. Imaging slow failure in triaxially deformed Etna basalt using 3D acoustic-emission location and X-ray computed tomography, *Geophysical Research Letters*, 10.1029/2006GL028721.

Benson, P. M., Vinciguerra, S., Meredith, P. G. and Young, R. P., 2008. Laboratory simulation of volcano seismicity, *Science*, **322**, 249-252.

Bonaccorso, A., 2004. Mount Etna: Volcano Laboratory, edited by Bonaccorso, A., Calvari, S., Coltelli, M., Del Negro, C. and Falsaperla, S., American Geophysical Union Geophysical Monograph 143.

Bonaccorso, A., Aloisi, M. and Mattia, M., 2002. Dike emplacement forerunning the Etna July 2001 eruption modeled through continuous tilt and GPS data, *Geophysical Research Letters*, **29**, No. 13, 1624, doi: 10.1029/2001GL014397.

Bonaccorso, A., Currenti, G., Del Negro, C. and Boschi, E., 2010. Dike deflection modelling for inferring magma pressure and withdrawal, with application to Etna 2001 case, *Earth and Planetary Science Letters*, **293**, 121-129.

ACCEPTED MANUSCRIPT

Bonforte, A., Gambino, S. and Neri, M., 2009. Intrusion of eccentric dikes: The case of the 2001 eruption and its role in the dynamics of Mt. Etna volcano, *Tectonophysics*, **471**, 78-86.

Bonforte, A. and Puglisi, G., 2006. Dynamics of the eastern flank of Mt. Etna volcano (Italy) investigated by a dense GPS network, *Journal of Volcanology and Geothermal Research*, **153**, 357-369.

Bonforte, A. and Puglisi, G., 2003. Magma uprising and flank dynamics on Mount Etna volcano, studied using GPS data (1994–1995), *Journal of Geophysical Research*, **108**, doi:10.1029/2002JB001845.

Borgia, A., Delaney, P. T. and Denlinger, R. P., 2000. Spreading volcanoes, *Annual Reviews in Earth and Planetary Sciences*, **28**, 539-570.

Borgia, A., Ferrari, L. and Pasquare, G., 1992. Importance of gravitational spreading in the tectonic and volcanic evolution of Mount Etna, *Nature*, **357**, 231-235.

Borgia, A., Lanari, R., Sansosti, E., Tesauro, M., Berardino, P., Fornaro, G., Neri, M. and Murray, J. B., 2000. Actively growing anticlines beneath Catania from the distal motion of Mount Etna's decollement measured by SAR interferometry and GPS, *Geophysical Research Letters*, **27**, 3409-3412.

Boynton, R. S., 1980. Chemistry and Technology of Lime and Limestone, 2nd edn. Wiley, New York.

Bruno, N., Caltabiano, T., Giammanco, S. and Romano, R., 2001. Degassing of SO2 and CO2 at Mount Etna (Silcily) as an indicator of pre-eruptive ascent and shallow emplacement of magma, *Journal of Volcanology and Geothermal Research*, **110**, 137-153.

Bruno, P. P. G., Cippitelli, G. and Rapolla, A., 1998. Seismic study of the Mesozoic carbonate basement around Mt. Somma–Vesuvius, Italy, *Journal of Volcanology and Geothermal Research*, **84**, 311-322.

Buick, I. S. and Cartwright, I., 2000. Fractured-controlled fluid flow and metasomatism in the contact aureole of the Marulan Batholith (New South Wales, Australia), *Contributions to Mineralogy and Petrology*, **143**, 733-749.

Burollet, P. F., 1991. Structures and tectonics of Tunisia, *Tectonophysics*, **195**, 359-369.

Carbone, D., D'Amico, S., Musumeci, C. and Greco, F., 2009. Comparison between the 1994–2006 seismic and gravity data from Mt. Etna: New insight into the long-term behavior of a complex volcano, *Earth and Planetary Science Letters*, **279**, 282-292.

Carrigan, C. R., Schubert, G. and Eichelberger, J. C., 1992. Thermal and Dynamical Regimes of Single- and Two-Phase Magmatic Flow in Dikes, *Journal of Geophysical Research*, **97**, 17377-17392.

Carslaw, H. S. and Jaeger, J. C., 1986. Conduction of Heat in Solids, Oxford University Press, Oxford, ISBN: 0198533683, 526 pages.

Catalano, S., Torrisi, S. and Ferlito, C., 2004. The relationship between Late Quaternary deformation and volcanism of Mt. Etna (eastern Sicily): new evidence from the sedimentary substratum in the Catania region, *Journal of Volcanology and Geothermal Research*, **132**, 311-334.

ACCEPTED MANUSCRIPT

Chadwick, J. P., Troll, V. R., Ginibre, C., Morga, D., Gertisser, R., Waight, T. E. and Davidson, J. P., 2007. Carbonate assimilation at Merapi Volcano, Java, Indonesia: insights from crystal isotope stratigraphy, *Journal of Petrology*, **48**, 1793-1812.

Chen, L.-J., He, J., Chao, J.-Q. and Qin, B.-D., 2009. Swelling and breaking characterisitics of limestone under high temperatures, *Mining Science and Technology*, 503-507.

Cheng, C. H. and Johnston, D. H., 1981. Dynamic and static moduli, *Geophysical Research Letters*, **8**, 39-42.

Chiarabba, C., Amato, A., Boschi, E. and Barberi, E., 2000. Recent seismicity and tomographic modeling of the Mount Etna plumbing system, *Journal of Geophysical Research*, **105**, 10923-10938.

Chiarabba, C., De Gori, P. and Patanè, D., 2004. The Mount Etna plumbing system: The contribution of seismic tomography, *in: Mount Etna volcano, Geophys. Monogr. Ser.*, vol. 143, edited by A. Bonoccorso et al., pp. 191-204, AGU, Washington, USA.

Chiodini, G., Caliro, S., Aiuppa, A., Avino, R., Granieri, D., Moretti, M. and Parello, F., 2011. First 13C/12C isotopic characterisation of volcanic plume CO2, *Bulletin of Volcanology*, doi: 10.1007/s00445-010-0423-2.

Chiodini, G. and Frondini, F., 2001. Carbon dioxide degassing from the Albani Hills volcanic region, Central Italy, *Chemical Geology*, **177**, 67-83.

Choi, N.-K., Kim, T.-W. and Rhee, K. Y., 2005. Kaiser effects in acoustic emission from composites during thermal cyclic-loading, *NDT & E International*, **38**, 268-274.

Ciccotti, M. and Mulargia, F., 2004. Differences between static and dynamic elastic moduli of a typical seismogenic rock, *Geophysical Journal International*, **157**, 474-477.

Ciccotti, M., Negri, N., Sassi, L., Gonzato, G. and Mulargia, F., 2000. Elastic and fracture parameters of Etna, Stromboli, and Vulcano lava rocks, *Journal of Volcanology and Geothermal Research*, **98**, 209-217.

D'Alessandro, W. D., Giammanco, S., Parello, F. and Valenza, M., 1997. CO_2 output and $\delta^{13}C(CO2)$ from Mount Etna as indicators of degassing of shallow asthenosphere *Bulletin of Volcanology*, **58**, 455-458.

D'Antonio, M., 2011. Lithology of the basement underlying the Campi Flegrei caldera: Volcanological and petrological constraints, *Journal of Volcanology and Geothermal Research*, **200**, 91-98.

David, C., Menéndez, B. and Darot, M., 1999. Infuence of stress-induced and thermal cracking on physical properties and microstructure of La Peyratte granite, *International Journal of Rock Mechanics and Mining Sciences*, **36**, 433-448.

Davidson, J. and De Silva, S. L., 2000. Composite Volcanoes, *In: Encyclopedia of Volcanoes (Edited by: Sigurdsson, H., B. Houghton, S. R. McNutt, H. Rymer and J. Stix)*, Academic Press.

Deegan, F. M., Troll, V. R., Freda, C., Misiti, V., Chadwick, J. P., McLeod, C. L. and Davidson, J. P., 2010. Magma–Carbonate Interaction Processes and Associated CO2 Release at Merapi Volcano, Indonesia: Insights from Experimental Petrology, *Journal of Petrology*, **51**, 1027-1061.

ACCEPTED MANUSCRIPT

Del Gaudio, P., Mollo, S., Ventura, G., Iezzi, G., Taddeucci, J. and Cavallo, A., 2010. Cooling rate-induced differentiation in anhydrous and hydrous basalts at 500 MPa: Implications for the storage and transport of magmas in dikes, *Chemical Geology*, **270**, 164-178.

Del Negro, C., Currenti, G. and Scandura, D., 2009. Temperature-dependent viscoelastic modeling of ground deformation: application to Etna volcano during the 1993–1997 inflation period., *Phys. Earth Planet. Inter.*, **172**, 299-309.

Delle Piane, C., Burlini, L. and Grobety, B., 2007. Reaction-induced strain localization: Torsion experiments on dolomite, *Earth and Planetary Science Letters*, **256**, 36-46.

Delle Piane, C., Burlini, L., Kunze, K., Brack, P. and Burg, J.-P., 2008. Rheology of dolomite: Large strain torsion experiments and natural examples, *Journal of Structural Geology*, **30**, 767-776.

Eberhardt, E., Stead, D. and Stimpson, B., 1999. Quantifying progressive pre-peak brittle fracture damage in rock during uniaxial compression, *International Journal of Rock Mechanics and Mining Sciences*, **36**, 361-380.

Eissa, E. A. and Kazi, A., 1989. Relation between static and dynamic Young's moduli of rocks, *International Journal of Rock Mechanics and Mining Sciences and Geomechanics Abstracts*, **25**, 479-482.

Elsworth, D. and Voight, B., 1996. Evaluation of volcano flank instability triggered by dyke intrusion, *Geol. Soc. London, Special Publications*, **110**, 45-53.

Evans, B., Fredrich, J. T. and Wong, T.-f., 1990. The brittle-ductile transition in rocks: recent experimental and theoretical progress, *in: The Brittle-Ductile Transition in Rocks, The Heard Volume (Eds: A. G. Duba, W. B. Durham, J. W. Handin, and H. F. Wang)*, ISBN: 0-87590-025-9, 1-20.

Faulkner, D. R., Mitchell, T. M., Healy, D. and Heap, M. J., 2006. Slip on 'weak' faults by the rotation of regional stress in the fracture damage zone, *Nature*, **444**, 922-925.

Finger, L. W., Cox, D. E. and Jephcoat, A. P., 1994. A correction for powder diffraction peak asymmetry due to axial divergence, *Journal of Applied Crystallography*, **27**, 892-900.

Fortin, J., Stantchits, S., Vinciguerra, S. and Guéguen, Y., 2010. Influence of thermal and mechanical cracks on permeability and elastic wave velocities in a basalt from Mt. Etna volcano subjected to elevated pressure, *Tectonophysics*, 10.1016/j.tecto.2010.09.028.

Freda, C., Gaeta, M., Misiti, V., Mollo, S., Dolfi, D. and Scarlato, P., 2008. Magma-carbonate interaction: an experimental study on ultrapotassic rocks from Alban Hills (Central Italy), *Lithos*, **101**, 397-415.

Fredrich, J. T. and Wong, T.-f., 1986. Micromechanics of thermally induced cracking in three crustal rocks, *Journal of Geophysical Research*, **91**, 12743-12764.

Frezzotti, M. L., Peccerillo, A. and Panza, G., 2009. Carbonate metasomatism and CO2 lithosphere–asthenosphere degassing beneath the Western Mediterranean: An integrated model arising from petrological and geophysical data, *Chemical Geology*, **262**, 108-120.

ACCEPTED MANUSCRIPT

Froger, J.-L., Merle, O. and Briole, P., 2001. Active spreading and regional extension at Mount Etna imaged by SAR interferometry, *Earth and Planetary Science Letters*, **187**, 245-258.

Gaeta, M., Di Rocco, T. and Freda, C., 2009. Carbonate Assimilation in Open Magmatic Systems: the Role of Melt-bearing Skarns and Cumulate-forming Processes, *Journal of Petrology*, **50**, 361-385.

Gaeta, M., Freda, C., Christensen, J. N., Dallai, L., Marra, F., Karner, D. B. and Scarlato, P., 2006. Time-dependent geochemistry of clinopyroxene from the Alban Hills (Central Italy): clues to the source and evolution of ultrapotassic magmas, *Lithos*, **86**, 330-346.

Gerlach, T. M., McGee, K. A., Elias, T., Sutton, A. J. and Doukas, M. P., 2002. Carbon dioxide emission rate of Kilauea Volcano: Implications for primary magma and the summit reservoir, *Journal of Geophysical Research*, **107**, 2189, doi:10.1029/2001JB000407.

Giammanco, S., Gurrieri, S. and Valenza, M., 1998. Anomalous soil CO_2 degassing in relation to faults and eruptive fissures on Mount Etna (Sicily, Italy) *Bulletin of Volcanology*, **60**, 252-259.

Glover, P. W. J., Baud, P., Darot, M., Meredith, P. G., Boon, S., A., LeRevelec, M., Zoussi, S. and Reuschle, T., 1995. α/β phase transition in quartz monitored using acoustic emissions., *Geophysical Journal International*, **120**, 775-782.

Goff, F., Love, S. P., Warren, R. G., Counce, D., Obenholzner, J., Siebe, C. and Schmidt, S. C., 2001. Passive infrared remote sensing evidence for large, intermittent CO2 emissions at Popocatépetl volcano, Mexico, *Chemical Geology*, **177**, 133-156.

Grasso, M. and Lentini, F., 1982. Sedimentary and tectonic evolution of the eastern Hyblean Plateau (southeastern Sicily) during late Cretaceous to Quaternary time, *Palaeogeography, Palaeoclimatology, Palaeoecology*, **39**, 261-280.

Griggs, D. T., Paterson, M. S., Heard, H. C. and Turner, F. J., 1960. Annealing recrystallization in calcite crystals and aggregates, *in: Rock Deformation, Memoir of the Geological Society of America (eds: D. T. Griggs and J. Handin)*, **79**, 21-37.

Gudmundsson, A., 2011. Deflection of dykes into sills at discontinuities and magma-chamber formation, *Tectonophysics*, **500**, 50-64.

Gudmundsson, A., 2004. Effects of Young's modulus on fault displacement, *C. R. Geodyamics*, **336**, 85-92.

Gudmundsson, A., 2009. Toughness and failure of volcanic edifices, *Tectonophysics*, **471**, 27-35.

Guéguen, Y. and Palciauskas, V., 1994. Introduction to the Physics of Rocks, Princeton University Press, ISBN: 9780691034522.

Gunasekaren, S. and Anbalagan, G., 2007. Thermal decomposition of natural dolomite, *Bulletin of Materials Science*, **30**, 339-344.

Gutenberg, B. and Richter, C. F., 1956. Magnitude and energy of earthquakes, *Annals of Geophysics (Rome)*, **9**, 1-15.

ACCEPTED MANUSCRIPT

Gutenberg, B. and Richter, C. F., 1955. Magnitude and energy of earthquakes, *Nature*, **176**, 795-796.

Heap, M. J., Baud, P., Meredith, P. G., Vinciguerra, S., Bell, A. F. and Main, I. G., 2011. Brittle creep in basalt and its application to time-dependent volcano deformation, *Earth and Planetary Science Letters*, **307**, 71-82.

Heap, M. J. and Faulkner, D. R., 2008. Quantifying the evolution of static elastic properties as crystalline rock approaches failure, *International Journal of Rock Mechanics and Mining Sciences*, **45**, 564-573.

Heap, M. J., Faulkner, D. R., Meredith, P. G. and Vinciguerra, S., 2010. Elastic moduli evolution and accompanying stress changes with increasing crack damage: implications for stress changes around fault zones and volcanoes during deformation, *Geophysical Journal International*, **183**, 225-236.

Heap, M. J., Lavallée, Y., Laumann, A., Hess, K.-U., Meredith, P. G. and Dingwell, D. B., 2012. How tough is tuff in the event of fire?, *Geology*, **40**, 311-314.

Heap, M. J., Vinciguerra, S. and Meredith, P. G., 2009. The evolution of elastic moduli with increasing crack damage during cyclic stressing of a basalt from Mt. Etna volcano, *Tectonophysics*, **471**, 153-160.

Heard, H. C. and Page, L., 1982. Elastic Moduli, Thermal Expansion, and Inferred Permeability of Two Granites to 350øC and 55 Megapascals, *Journal of Geophysical Research*, **87**, 9340-9348.

Hess, K.-U., Cordonnier, B., Lavallée, Y. and Dingwell, D. B., 2007. High-load, high-temperature deformation apparatus for synthetic and natural silicate melts, *Review of Scientific Instruments*, 10.1063/1.2751398.

Hoek, E. and Brown, E. T., 1997. Practical estimates of rock mass strength, *International Journal of Rock Mechanics and Mining Sciences*, **34**, 1165-1186.

Homand-Etienne, F. and Houpert, R., 1989. Thermally induced microcracking in granite: characterisation and analysis, *International Journal of Rock Mechanics and Mining Sciences and Geomechanics Abstracts*, **26, No. 2**, 125-134.

Homand-Etienne, F. and Troalen, J.-P., 1984. Behaviour of granites and limestones subjected subjected to slow and homogenous temperature changes, *Engineering Geology*, **20**, 219-233.

Iacono-Marziano, G., Gaillard, F. and Pichavant, M., 2007. Limestone assimilation and the origin of CO2 emissions at the Alban Hills (Central Italy): Constraints from experimental petrology, *Journal of Volcanology and Geothermal Research*, **166**, 91-105.

Iacono-Marziano, G., Gaillard, F., Scaillet, B., Pichavant, M. and Chiodini, G., 2009. Role of non-mantle CO2 in the dynamics of volcano degassing: The Mount Vesuvius example, *Geology*, **37**, 319-322.

Kennedy, L. and Cleven, N., 2011. The role of dolomite content on the mechanical strength in dolomite-limestone composites, *Geophysical Research Abstracts*, **13**, EGU2011-13003.

Kilburn, C. R. J., 2003. Multiscale fracturing as a key to forecasting volcanic eruptions *Journal of Volcanology and Geothermal Research*, **125**, 271-289.

ACCEPTED MANUSCRIPT

Kilburn, C. R. J. and Sammonds, P. R., 2005. Maximum warning times for imminent volcanic eruptions, *Geophysical Research Letters*, 10.1029/2005GL024184.

Kök, M. V. and Smykatz-Kloss, W., 2001. Thermal Characterization of Dolomites, *Journal of Thermal Analysis and Calorimetry*, **64**, 1271-1275.

Laigle, M., Hirn, A., Sapin, M., Lépine, J.-C., Diaz, J., Gallart, J. and Nicolich, R., 2000. Mount Etna dense array local earthquake P and S tomography and implications for volcanic plumbing, *Journal of Geophysical Research*, **105**, 21633-21646.

Lanari, R., De Natale, G., Berardino, P., Sansosti, E., Ricciardi, G. P., Borgstrom, S., Capuano, P., Pingue, F. and Troise, C., 2002. Evidence for a peculiar style of ground deformation inferred at Vesuvius volcano, *Geophysical Research Letters*, **29**, No. 9, 1292, doi: 10.1029/2001GL014571.

Larson, A. C. and von Dreele, R. B., 1997. GSAS: General Structure Analysis System, *Document LAUR 86-748*, Los Alamos National Laboratory.

Lau, J. S. O. and Chandler, N. A., 2004. Innovative laboratory testing, *International Journal of Rock Mechanics and Mining Sciences*, **41**, 1427-1445.

Le Bail, A., 2005. Whole powder pattern decomposition methods and applications - a retrospection, *Powder Diffraction*, **20**, 316-326.

Lentini, F., 1982. The geology of the Mt. Etna basement, *Mem. Soc. Geol. Ital., XXIII*, **23**, 7-25.

Li, C.-T. and Albe, W. R., 1993. Development of an improved XRD sample holder, *Powder Diffraction*, **8**, 118-121.

Li, M. Q. and Messing, G. L., 1983. Chloride salt effects on the decomposition of dolomite, *Thermochimica Acta*, **68**, 1-8.

Lundgren, P., Casu, F., Manzo, M., Pepe, A., Berardino, P., Sansosti, E. and Lanari, R., 2004. Gravity and magma induced spreading of Mount Etna volcano revealed by satellite radar interferometry, *Geophysical Research Letters*, **31**, L04602, doi:10.1029/2003GL018736.

Main, I. G., Meredith, P. G. and Jones, C., 1989. A reinterpretation of the precursory seismic b-value anomaly from fracture mechanics, *Geophysical Journal International*, **96**, 131-138.

Maitra, S., Choudhury, A., Das, H. S. and Pramanik, J., 2005. Effect of compaction on the kinetics of thermal decomposition of dolomite under non-isothermal condition, *Journal of Material Science*, **40**, 4749-4751.

Manconi, A., Walter, T. R. and Amelung, F., 2007. Effects of mechanical layering on volcano deformation, *Geophysical Journal International*, **170**, 952-958.

Manconi, A., Walter, T. R., Manzo, M., Zeni, G., Tizzani, P., Sansosti, E. and Lanari, R., 2010. On the effects of 3D mechanical heterogeneities at Campi Flegrei caldera, southern Italy, *Journal of Geophysical Research*, 10.1029/2009JB007099.

ACCEPTED MANUSCRIPT

Mao, X.-B., Zhang, L.-Y., Li, T.-Z. and Liu, H.-S., 2009. Properties of failure mode and thermal damage for limestone at high temperatures, *Mining Science and Technology*, 290-294.

Marsh, B. D., 1995. Solidification fronts and magmatic evolution, *Mineralogy Magazine*, **60**, 5-40.

McClauley, R. A. and Johnson, L. A., 1991. Decrepitation and thermal decomposition of dolomite, *Thermochimica Acta*, **185**, 271-282.

McGuire, W. J., 1996. Volcano instability: a review of contemporary themes, *Geol. Soc. London*, **110**, 1-23.

McIntosh, R. M., Sharp, J. H. and Wilburn, F. W., 1990. The thermal decomposition of dolomite, *Thermochimica Acta*, **165**, 281-296.

Menéndez, B., David, C. and Darot, M., 1999. A Study of the Crack Network in Thermally and Mechanically Cracked Granite Samples using Confocal Scanning Laser Microscopy, *Phys. Chem. Earth*, **24, No. 7**, 627-632.

Meredith, P. G., Main, I. G. and Jones, C., 1990. Temporal variations in seismicity during quasi-static and dynamic rock failure, *Tectonophysics*, **175**, 249-268.

Merle, O. and Borgia, A., 1996. Scaled experiments of volcanic spreading, *Journal of Geophysical Research*, **101**, No. B6, 13805-13817.

Métrich, N. and Rutherford, M. J., 1998. Low pressure crystallization paths of H2O-saturated basaltic-hawaiitic melts from Mt Etna: Implications for open-system degassing of basaltic volcanoes, *Geochimica et Cosmochimica Acta*, **62**, 1195-1205.

Michaud, V., 1995. Crustal xenoliths in recent hawaiites from Mount Etna, Italy: evidence for alkali exchanges during magma-wall rock interaction, *Chemical Geology*, **122**, 21-42.

Mollo, S., Del Gaudio, P., Ventura, G., Iezzi, G. and Scarlato, P., 2010a. Dependence of clinopyroxene composition on cooling rate in basaltic magmas: Implications for thermobarometry, *Lithos*, **118**, 302-312.

Mollo, S., Gaeta, M., Freda, C., Di Rocco, T., Misiti, V. and Scarlato, P., 2010b. Carbonate assimilation in magmas: A reappraisal based on experimental petrology, *Lithos*, **114**, 503-514.

Mollo, S., Heap, M. J., Iezzi, G., Hess, K.-U., Scarlato, P. and Dingwell, D. B., 2012. Volcanic edifice weakening via decarbonation: a self-limiting process?, *Geophysical Research Letters*, **36**, L15307, doi: 10.1029/2012GL052613.

Mollo, S., Misiti, V. and Scarlato, P., 2010c. Trace element behaviour during interaction between basalt and crustal rocks at 0.5-0.8 GPa: an experimental approach, *Central European Journal of Geosciences*, **2 (2)**, 188-198.

Mollo, S., Putirka, K., Iezzi, G., Del Gaudio, P. and Scarlato, P., 2011a. Plagioclase-melt (dis)equilibrium due to cooling dynamics: implications for thermometry, barometry and hygrometry, *Lithos*, doi:10.1016/j.lithos.2011.02.008.

ACCEPTED MANUSCRIPT

Mollo, S., Vinciguerra, S., Iezzi, G., Iarocci, A., Scarlato, P., Heap, M. J. and Dingwell, D. B., 2011b. Volcanic edifice weakening via devolatilization reactions, *Geophysical Journal International*, **186**, 1073-1077.

Murru, M., Montuori, C., Wyss, M. and Privitera, E., 1999. The locations of magma chambers at Mt. Etna, Italy, mapped by b-values, *Geophysical Research Letters*, **26**, No. 16, 2553-2556.

Neri, M., Acocella, V. and Behncke, B., 2004. The role of the Pernicana Fault System in the spreading of Mt. Etna (Italy) during the 2002–2003 eruption, *Bulletin of Volcanology*, **66**, 417-430.

Norini, G., Capra, L., Groppelli, G., Agliardi, F., Pola, A. and Cortes, A., 2010. Structural architecture of the Colima Volcanic Complex, *Journal of Geophysical Research*, **115**, B12209, doi:10.1029/2010JB007649.

Nur, A. M. and Simmons, G., 1969. The effect of saturation on velocity in low porosity rocks, *Earth and Planetary Science Letters*, **7**, 183-193.

O'Connell, R. J. and Budiansky, B., 1974. Seismic velocities in dry and saturated cracked solids, *Journal of Geophysical Research*, **79**, 5412-5426.

Palano, M., Gresta, S. and Puglisi, G., 2009. Time-dependent deformation of the eastern flank of Mt. Etna: After-slip or viscoelastic relaxation?, *Tectonophysics*, **473**, 300-311.

Palano, M., Puglisi, G. and Gresta, S., 2008. Ground deformation patterns at Mt. Etna from 1993 to 2000 from joint use of InSAR and GPS techniques, *Journal of Volcanology and Geothermal Research*, **169**, 99-120.

Pan, V., Holloway, J. R. and Hervig, R. L., 1991. The pressuer and temperature dependence of carbon dioxide solubility in tholeiitic basalt melts, *Geochimica et Cosmochimica Acta*, **55**, 1587-1595.

Papale, P., 1999. Modeling of the solubility of a two-component H2O + CO2 fluid in silicate liquids, *American Mineralogist*, **84**, 477-492.

Patanè, D., Barberi, G., Cocina, O., De Gori, P. and Chiarabba, C., 2006. Time-Resolved Seismic Tomography Detects Magma Intrusions at Mount Etna, *Science*, **313**, 821-823.

Patanè, D., Chiarabba, C., Cocina, O., De Gori, P., Moretti, M. and Boschi, E., 2002. Tomographic images and 3D earthquake locations of the seismic swarm preceding the 2001 Mt. Etna eruption: Evidence for a dyke intrusion, *Geophysical Research Letters*, **29**, No. 10, 1497, doi: 10.1029/2001GL014391.

Pedley, H. M., 1981. Sedimentology and palaeoenvironment of the southeast Sicilian Tertiary platform carbonates, *Sedimentary Geology*, **28**, 273-291.

Pedley, H. M. and Grasso, M., 1992. Miocene syntectonic sedimentation along the western margins of the Hyblean-Malta platform: A guide to plate margin processes in the central Mediterranean, *Journal of Geodynamics*, **15**, 19-37.

Percharsky, V. K. and Zavaliji, P. Y., 2005. Fundamentals of powder diffraction and structural characterization of materials, *Springer Science*, 713 pp.

ACCEPTED MANUSCRIPT

Petrakova, L., Heap, M. J., Lavallée, Y., Baud, P. and Dingwell, D. B., 2012. The effect of thermal stresses on the strength and physical properties of edifice-forming andesites: the case study of Volcan de Colima, *Journal of Volcanology and Geothermal Research*, submitted.

Piochi, M., Ayuso, R. A., De Vivo, B. and Somma, R., 2006. Crustal contamination and crystal entrapment during polybaric magma evolution at Mt. Somma-Vesuvius volcano, Italy: geochemical and Sr isotope evidence, *Lithos*, **86**, 303-329.

Rocchi, V., Sammonds, P. R. and Kilburn, C. R. J., 2004. Fracturing of Etnean and Vesuvian rocks at high temperatures and low pressures, *Journal of Volcanology and Geothermal Research*, **132**, 137-157.

Roman, D. C. and Cashman, K. V., 2006. The origin of volcano-tectonic earthquake swarms, *Geology*, **34**, 457-460.

Rust, D., Behncke, B., Neri, M. and Ciocanel, A., 2005. Nested zones of instability in the Mount Etna volcanic edifice, Italy, *Journal of Volcanology and Geothermal Research*, **144**, 137-153.

Rutter, E., 1974. The influence of temperature, strain rate and interstitial water in the deformation of calcite rocks, *Tectonophysics*, **22**, 331-334.

Rutter, E., 1986. On the nomenclature of mode of failure transitions in rocks, *Tectonophysics*, **122**, 381-387.

Rutter, E. H., 1972. The Effects of Strain-Rate Changes on the Strength and Ductility of Solenhofen Limestone at Low Temperatures and Confining Pressures, *International Journal of Rock Mechanics and Mining Sciences and Geomechanics Abstracts*, **1972**, 183-189.

Sammonds, P. R., Meredith, P. G. and Main, I. G., 1992. Role of pore fluids in the generation of seismic precursors to shear fracture, *Nature*, **359**, 228-230.

Samtani, M., Dollomore, D. and Alexander, K. S., 2002. Comparison of dolomite decomposition kinetics with related carbonates and the effect of procedural variables on its kinetic parameters, *Thermochimica Acta*, **392-393**, 135-145.

Schmidt, S. C., Paterson, M. S. and Boland, J. N., 1980. Hightemperature flow and dynamic recrystallization in carrara marble, *Tectonophysics*, **65**, 245-280.

Siebert, L., 1992. Threats from debris avalanches, *Nature*, **356**, 658-659.

Simmons, G. and Brace, W. F., 1965. Comparison of static and dynamic measurements of compressibility of rocks, *Journal of Geophysical Research*, **70**, 5649-5656.

Siniscalchi, A., Tripaldi, S., Neri, M., Giammanco, S., Piscitelli, S., Balasco, M., Behncke, B., Magri, C., Naudet, V. and Rizzo, E., 2010. Insights into fluid circulation across the Pernicana Fault (Mt. Etna, Italy) and implications for flank instability, *Journal of Volcanology and Geothermal Research*, **193**, 137-142.

Smith, R., Sammonds, P. R. and Kilburn, C. R. J., 2009. Fracturing of volcanic systems: Experimental insights into pre-eruptive conditions, *Earth and Planetary Science Letters*, **280**, 221-219.

ACCEPTED MANUSCRIPT

Stanchits, S., Vinciguerra, S. and Dresen, G., 2006. Ultrasonic Velocities, Acoustic Emission Characteristics and Crack Damage of Basalt and Granite, *Pure and Applied Geophysics*, **163**, 975-994.

Stolper, E. and Holloway, J. R., 1988. Experimental determination of the solubility of carbon dioxide in moltern basalt at low pressure, *Earth and Planetary Science Letters*, **87**, 397-408.

Szakács, A. and Krézsek, C., 2006. Volcano–basement interaction in the Eastern Carpathians: Explaining unusual tectonic features in the Eastern Transylvanian Basin, Romania, *Journal of Volcanology and Geothermal Research*, **158**, 6-20.

Tanguy, J. C., Condomines, M. and Kieffer, G., 1997. Evolution of the Mount Etna magma: Constraints on the present feeding system and eruptive mechanism, *Journal of Volcanology and Geothermal Research*, **75**, 221-250.

Tibaldi, A. and Groppelli, G., 2002. Volcano-tectonic activity along structures of the unstable NE flank of Mt. Etna (Italy) and their possible origin *Journal of Volcanology and Geothermal Research*, **115**, 277-302.

Toby, B. H., 2001. EXPGUI, a graphical user interface for GSAS, *Journal of Applied Crystallography*, **34**, 210-213.

Toksöz, M. N., Cheng, C. H. and Timur, A., 1976. Velocities of seismic waves in porous rocks, *Geophysics*, **41**, 621-645.

Troll, V. R., Hilton, D. R., Jolis, E. M., Chadwick, J. P., Blythe, L. S., Deegan, F. M., Schwarzkopf, L. M. and Zimmer, M., 2012. Crustal CO2 liberation during the 2006 eruption and earthquake events at Merapi volcano, Indonesia, *Geophysical Research Letters*, **39**, L11302, doi:10.1029/2012GL051307.

Turner, F. J., Griggs, D. T. and Heard, H., 1954. Experimental deformation of calcite crystals, *Geological Society of America Bulletin*, **65**, 883-934.

Van Wyk De Vries, B. and Borgia, A., 1996. The role of basement in volcano deformation, *Geol. Soc. London, Special Publications*, **110**, 95-110.

Van Wyk De Vries, B. and Francis, P. W., 1997. Catastrophic collapse at stratovolcanoes induced by gradual volcano spreading, *Nature*, **387**, 387-390.

Vinciguerra, S., Trovato, C., Meredith, P. G. and Benson, P. M., 2005. Relating seismic velocities, thermal cracking and permeability in Mt. Etna and Iceland basalts, *International Journal of Rock Mechanics and Mining Sciences*, **42**, 900-910.

Voight, B., 1989. A Relation to Describe Rate-Dependent Material Failure, *Science*, **243**, 200-203.

Walter, T. R., Acocella, V., Neri, M. and Amelung, F., 2005. Feedback processes between magmatic events and flank movement at Mount Etna (Italy) during the 2002–2003 eruption, *Journal of Geophysical Research*, 10.1029/2005JB003688.

Walter, T. R. and Troll, V. R., 2003. Experiments on rift zone evolution in unstable volcanic edifices, *Journal of Volcanology and Geothermal Research*, **127**, 107-120.

ACCEPTED MANUSCRIPT

Wang, X.-q., Schubnel, A., Fortin, J., David, E. C., Guéguen, Y. and Ge, H.-k., 2012. High Vp/Vs ratio: Saturated cracks or anisotropy effects?, *Geophysical Research Letters*, **39**, L11307, doi:10.1029/2012GL051742.

Wenzel, T., Baumgartner, L., Bruugmann, G. E., Konnikov, E. G. and Kislov, E., 2002. Partial melting and assimilation of dolomitic xenoliths by mafic magma: the Ioko-Dovyren intrusion (North Baikal Region, Russia). *Journal of Petrology*, **43**, 2049-2074.

Werner, C. and Brantley, S., 2003. CO2 emissions from the Yellowstone volcanic system, *Geochemistry, Geophysics and Geosystems*, **4**, 1061, doi: 10.1029/2002GC000473.

Xiao, X., Zhu, W. and Evans, B., 2003. Deformation mechanisms and failure modes in Solnhofen limestone, *12th Panamerican conference on soil mechanics and geotechnical engineering*, **1**, 39th U. S. Rock Mechanics Symposium.

Yellin-Dror, A., Grasso, M., Ben-Avraham, Z. and Tibor, G., 1997. The subsidence history of the northern Hyblean plateau margin, southeastern Sicily, *Tectonophysics*, **282**, 277-289.

Yong, C. and Wang, C.-Y., 1980. Thermally induced acoustic emission in Westerly granite, *Geophysical Research Letters*, **7, No. 12**, 1089-1092.

Young, R. A., 1993. The Rietveld method, *IUCr Monographs on crystallography*, Oxford University Press, 298 pp.

Zernack, A. V., Cronin, S. J., Bebbington, M. S., Price, R. C., Smith, I. E. M., Stewart, R. B. and Procter, J. N., 2012. Forecasting catastrophic stratovolcano collapse: A model based on Mount Taranaki, New Zealand, *Geology*, doi:10.1130/G33277.1.

Zhang, H., Thurber, C. and Bedrosian, P., 2009. Joint inversion for Vp, Vs, and Vp/Vs at SAFOD, Parkfield, California, *Geochemistry, Geophysics and Geosystems*, 10.1029/2009GC002709.

Zuberek, W. M., Zogala, B., Dubiel, R. and Pierwola, J., 1999. Maximum Temperature Memory in Sandstone and Mudstone Observed with Acoustic Emission and Ultrasonic Measurements, *International Journal of Rock Mechanics and Mining Sciences and Geomechanics Abstracts*, **35, No. 4/5**, 416-417.

ACCEPTED MANUSCRIPT

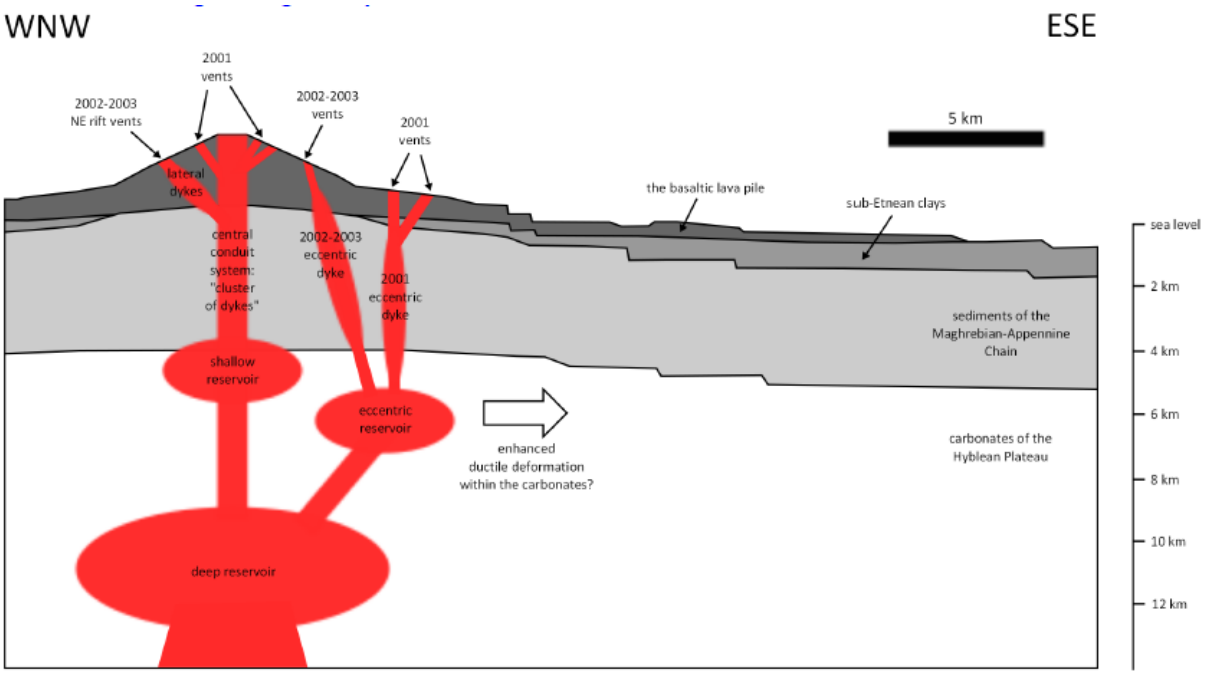

Fig. 1

ACCEPTED

ACCEPTED MANUSCRIPT

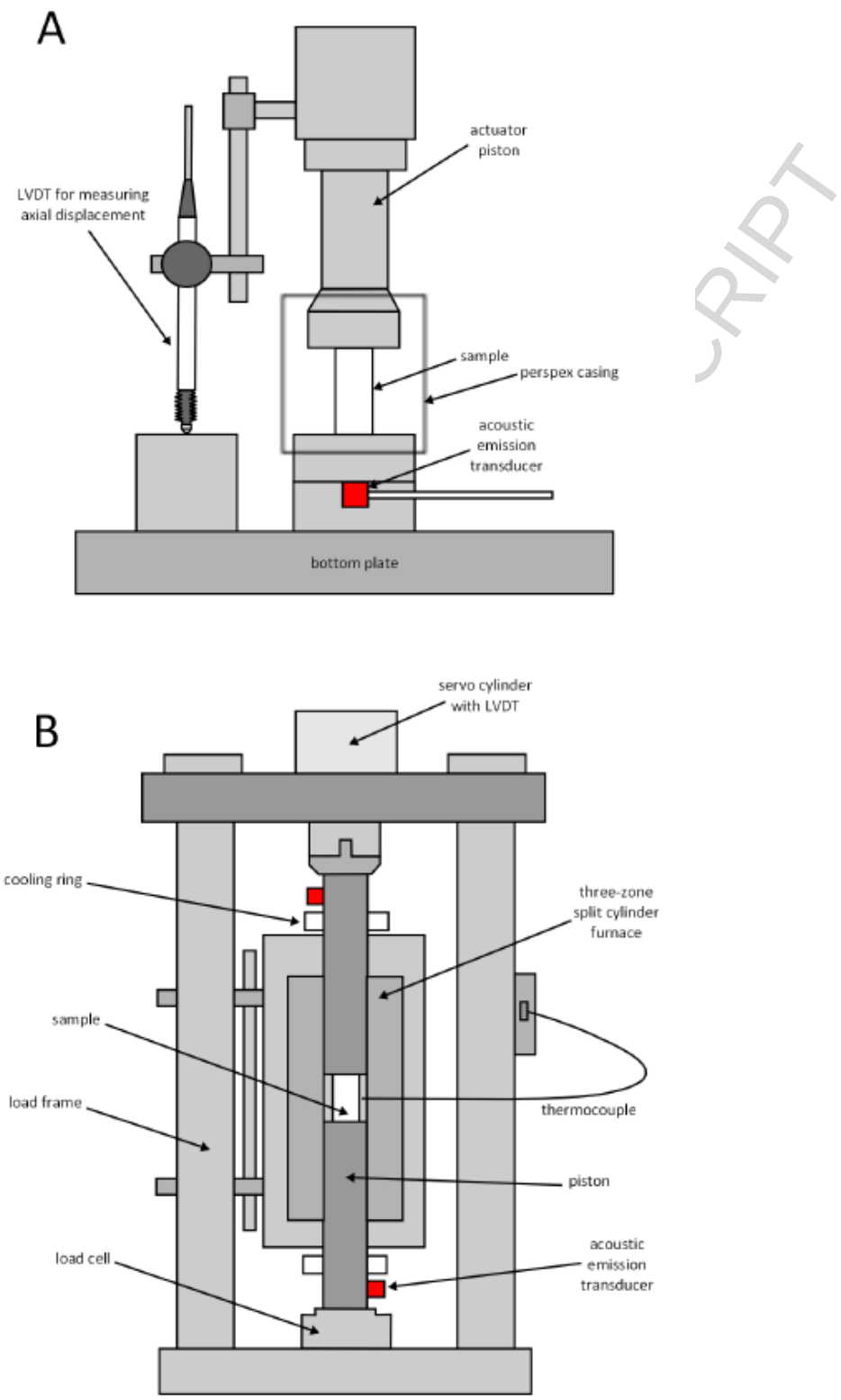

Fig. 2

ACCEPTED MANUSCRIPT

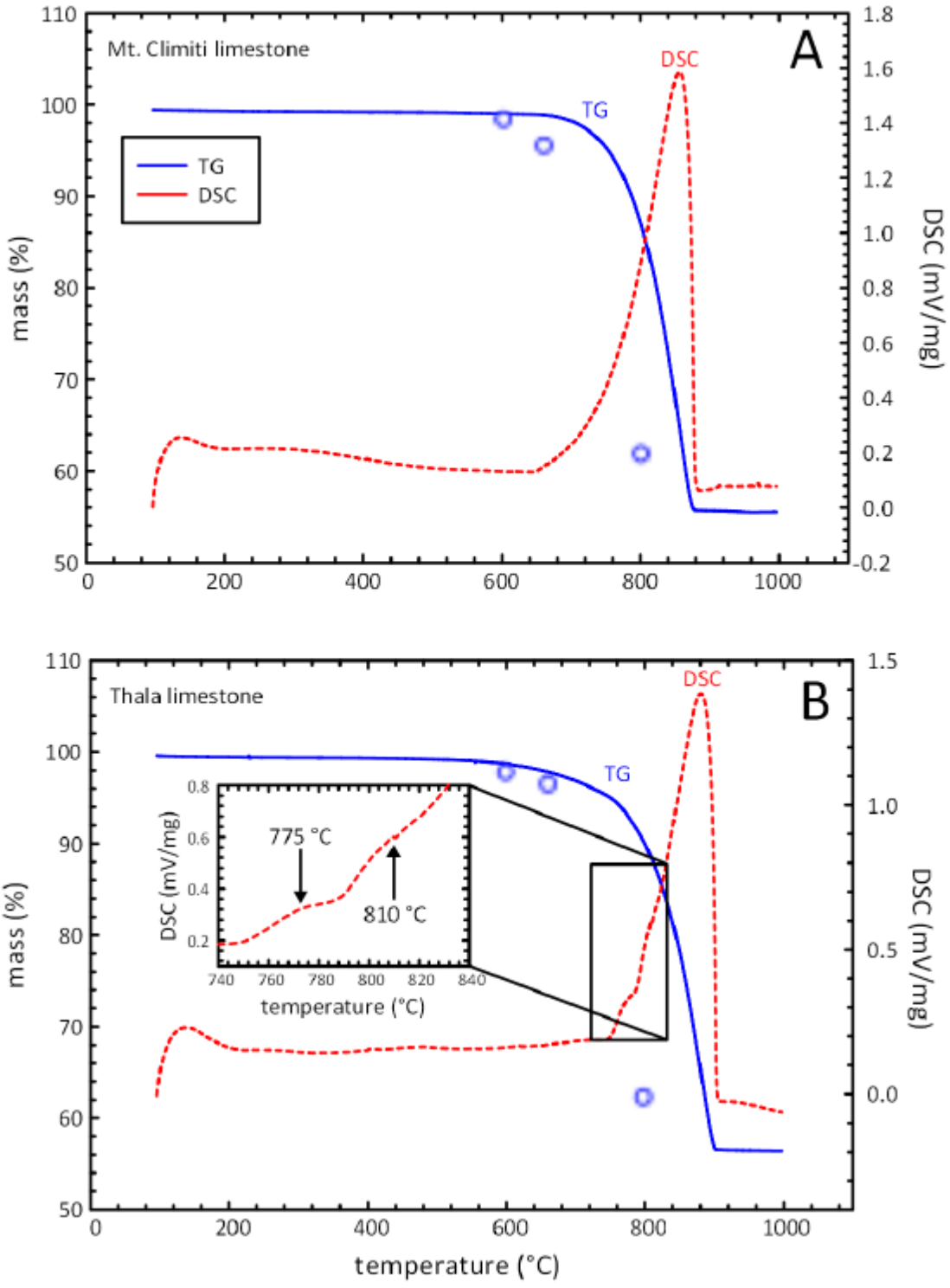

Fig. 3

ACCEPTED MANUSCRIPT

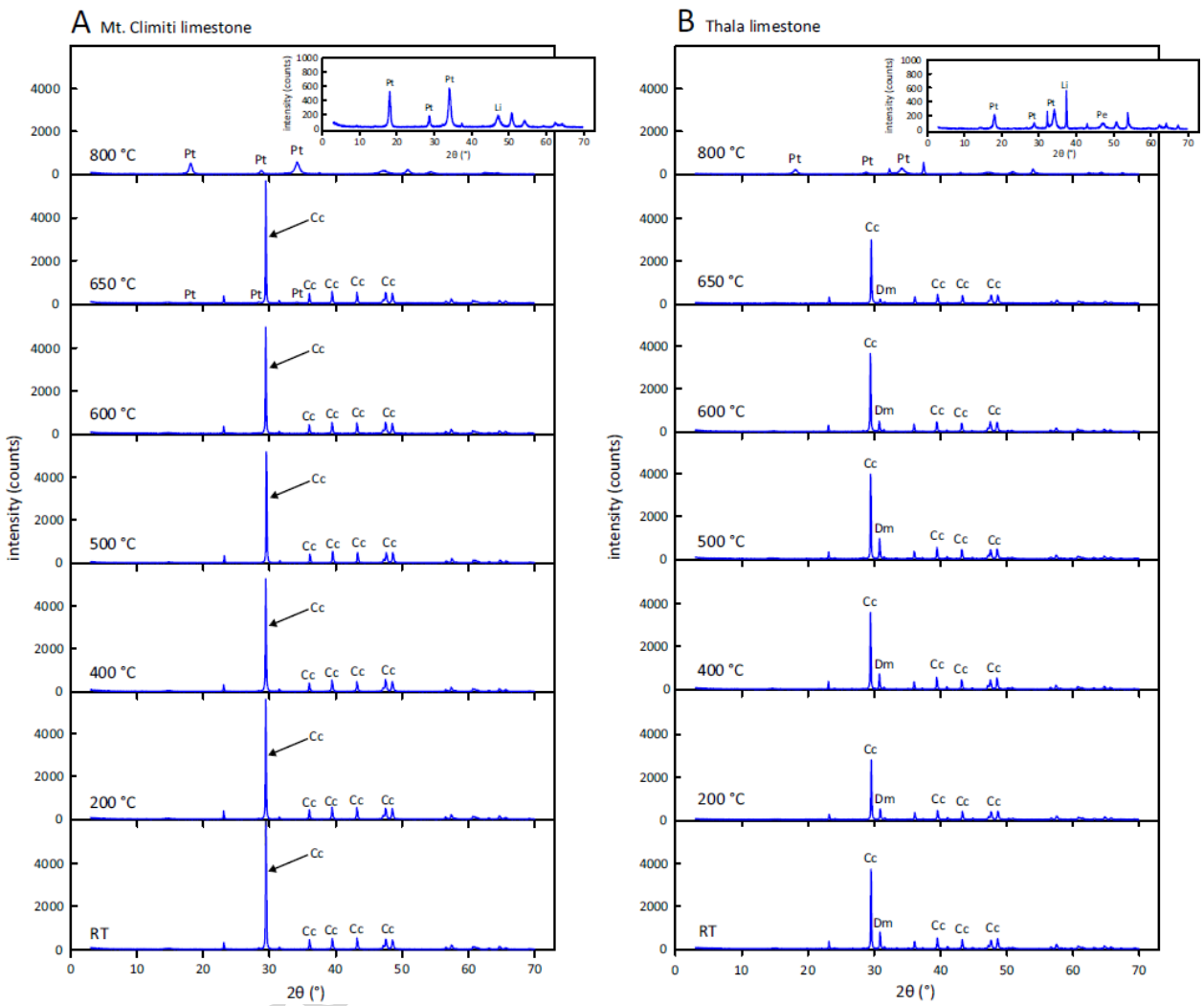

Fig. 4

ACCEPTED MANUSCRIPT

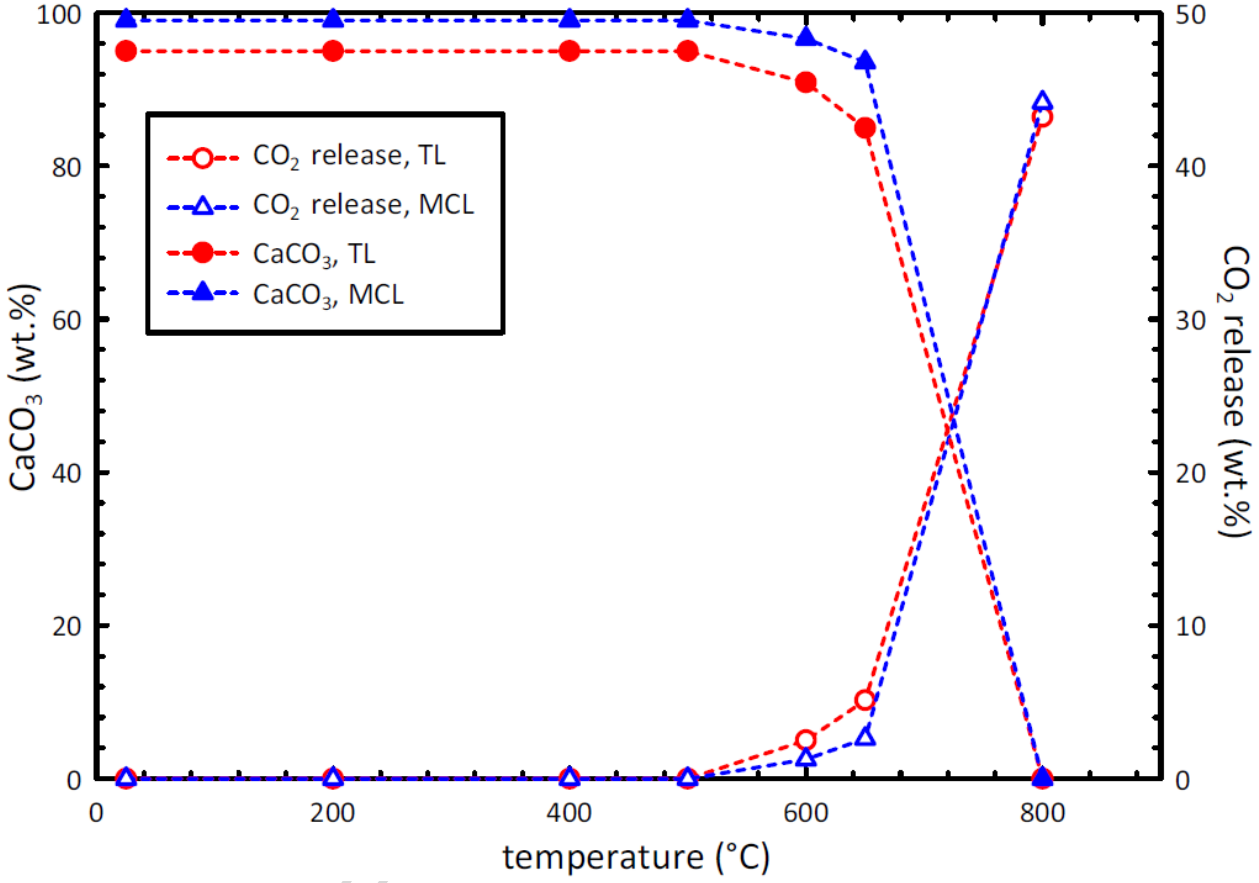

Fig. 5

ACCE

ACCEPTED MANUSCRIPT

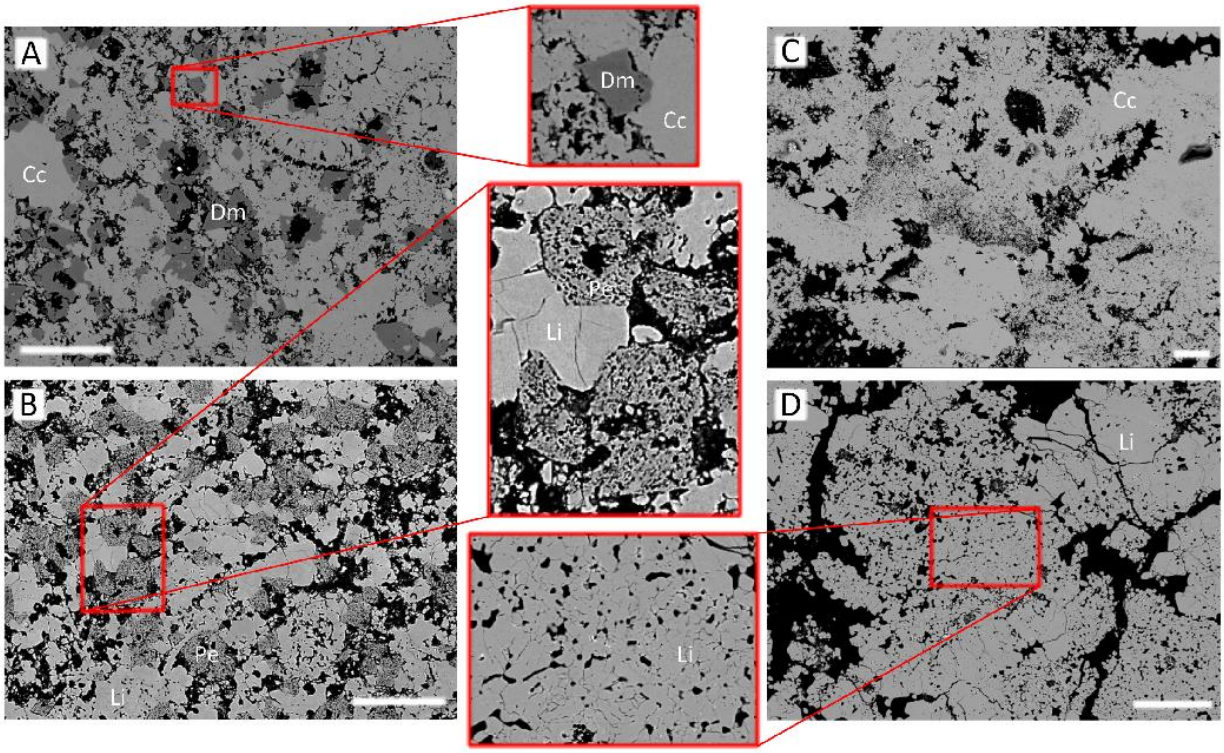

Fig. 6

ACCEPTED

ACCEPTED MANUSCRIPT

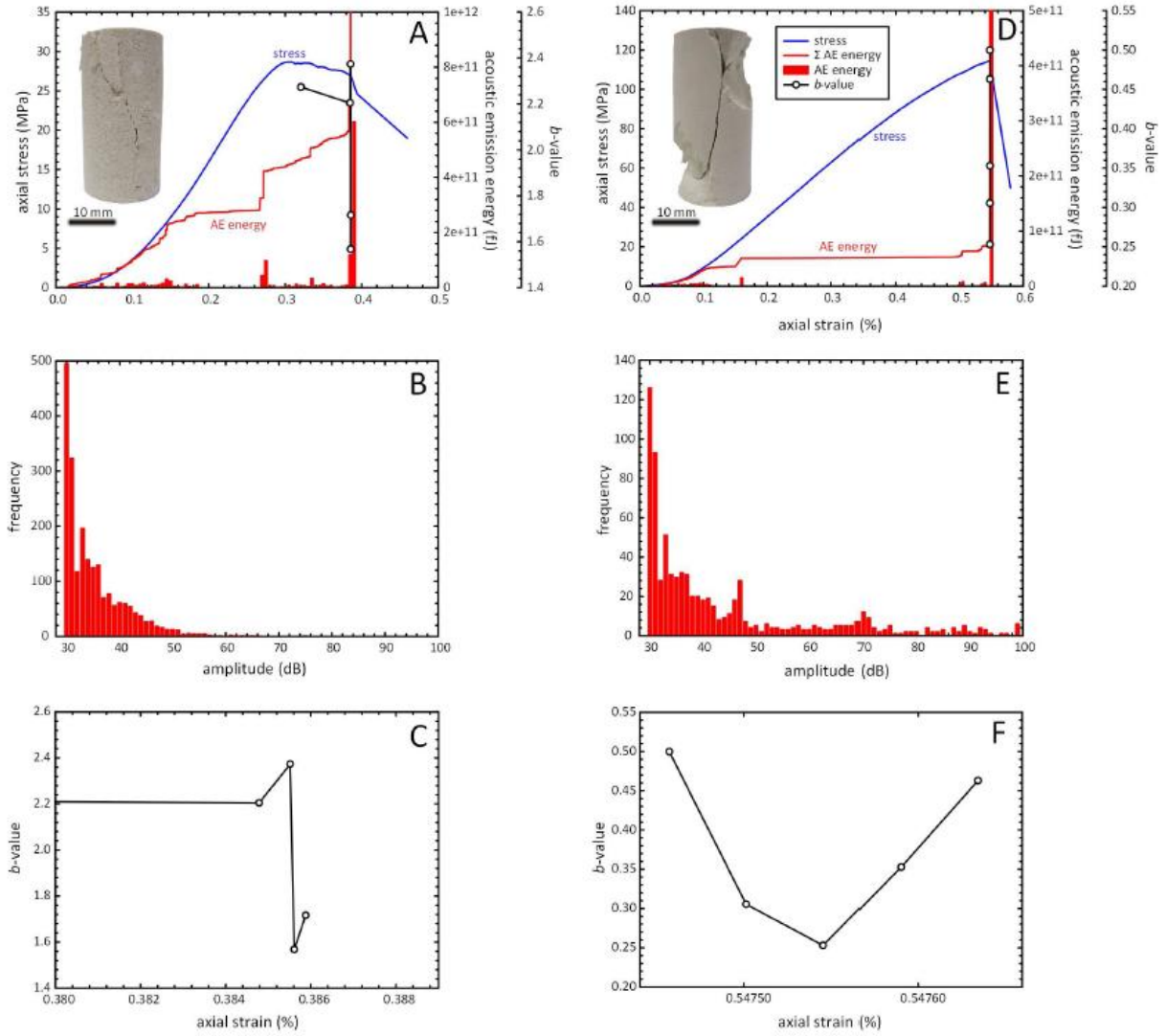

Fig. 7

ACCEPTED MANUSCRIPT

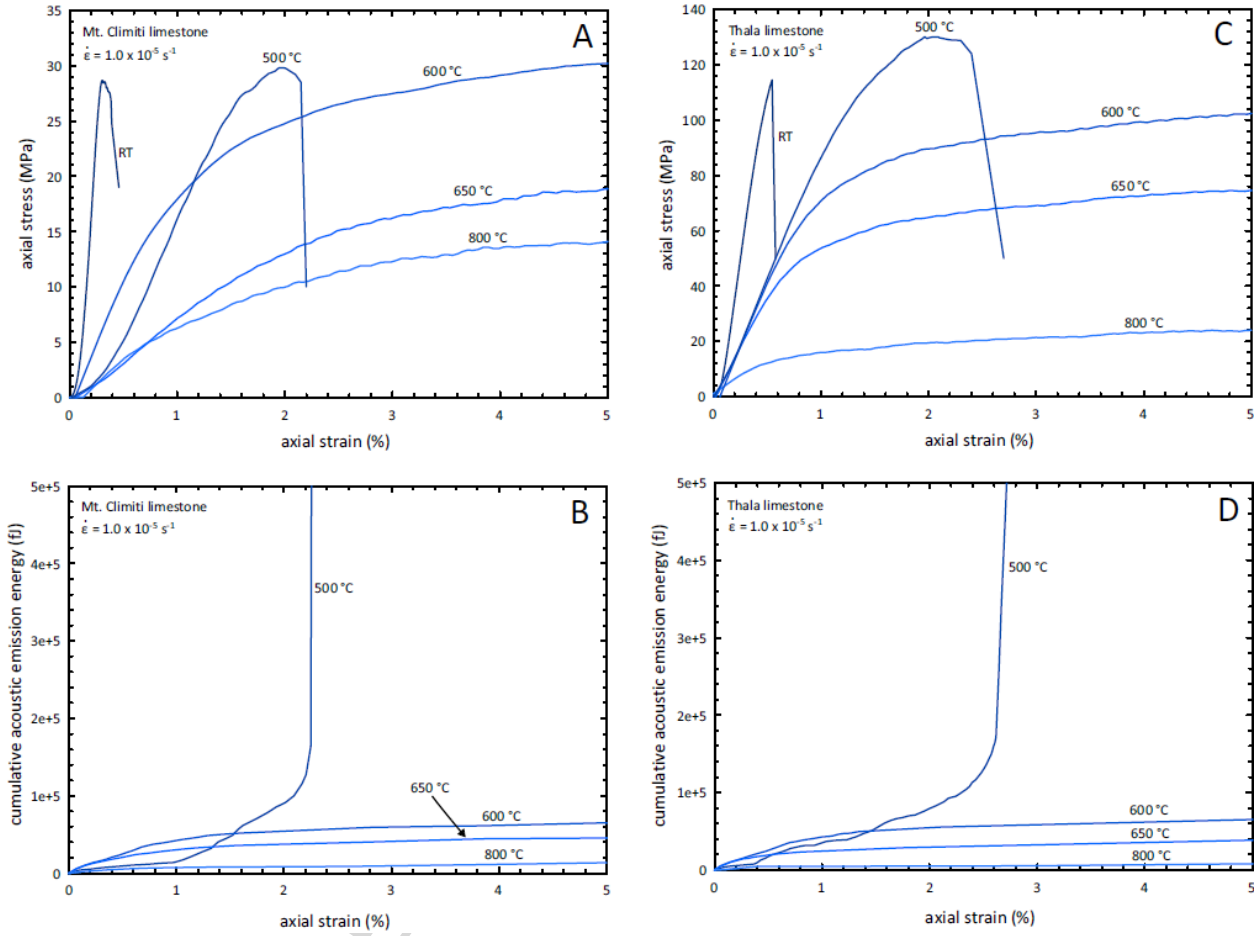

Fig. 8

ACCEPTED MANUSCRIPT

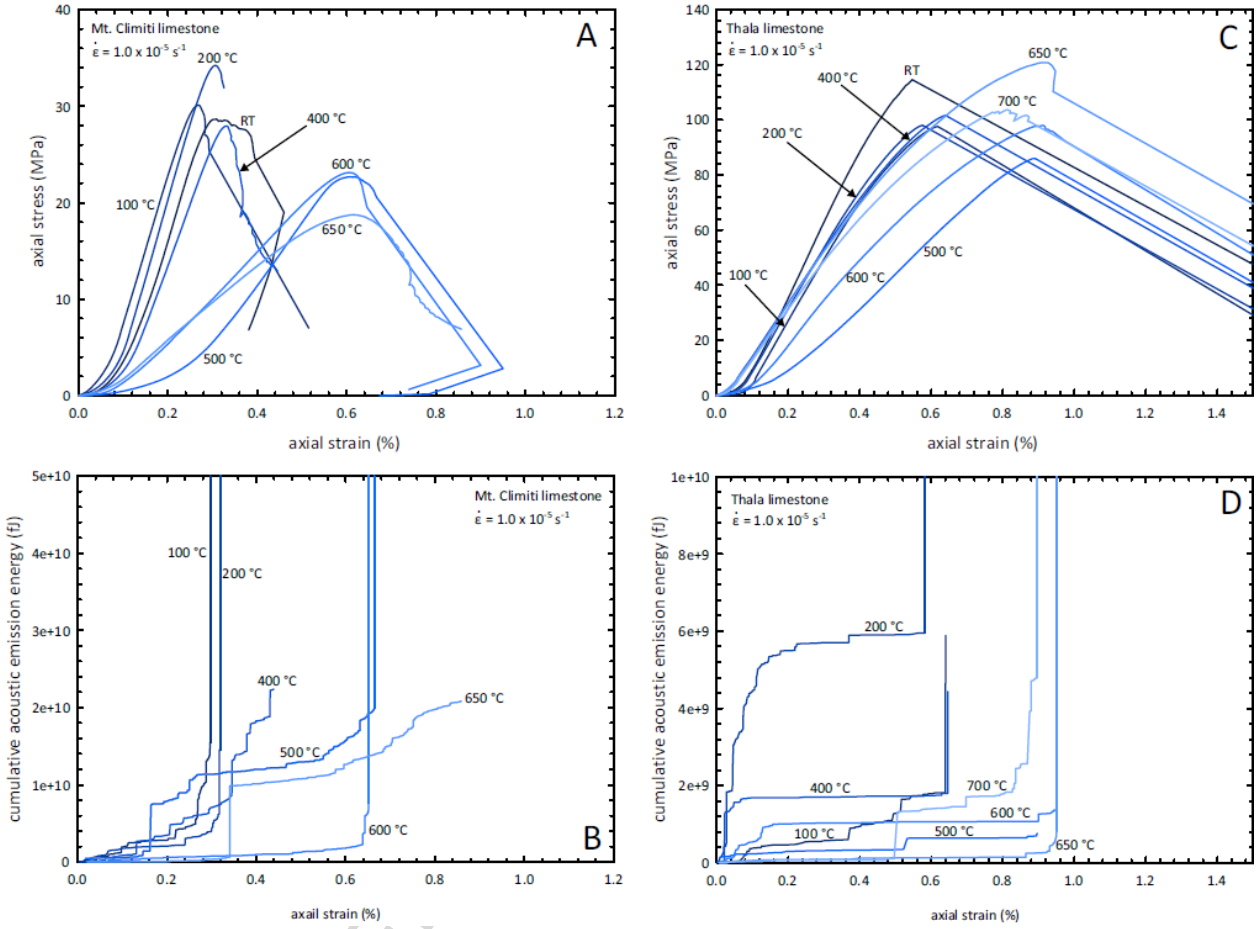

Fig. 9

ACCEPTED MANUSCRIPT

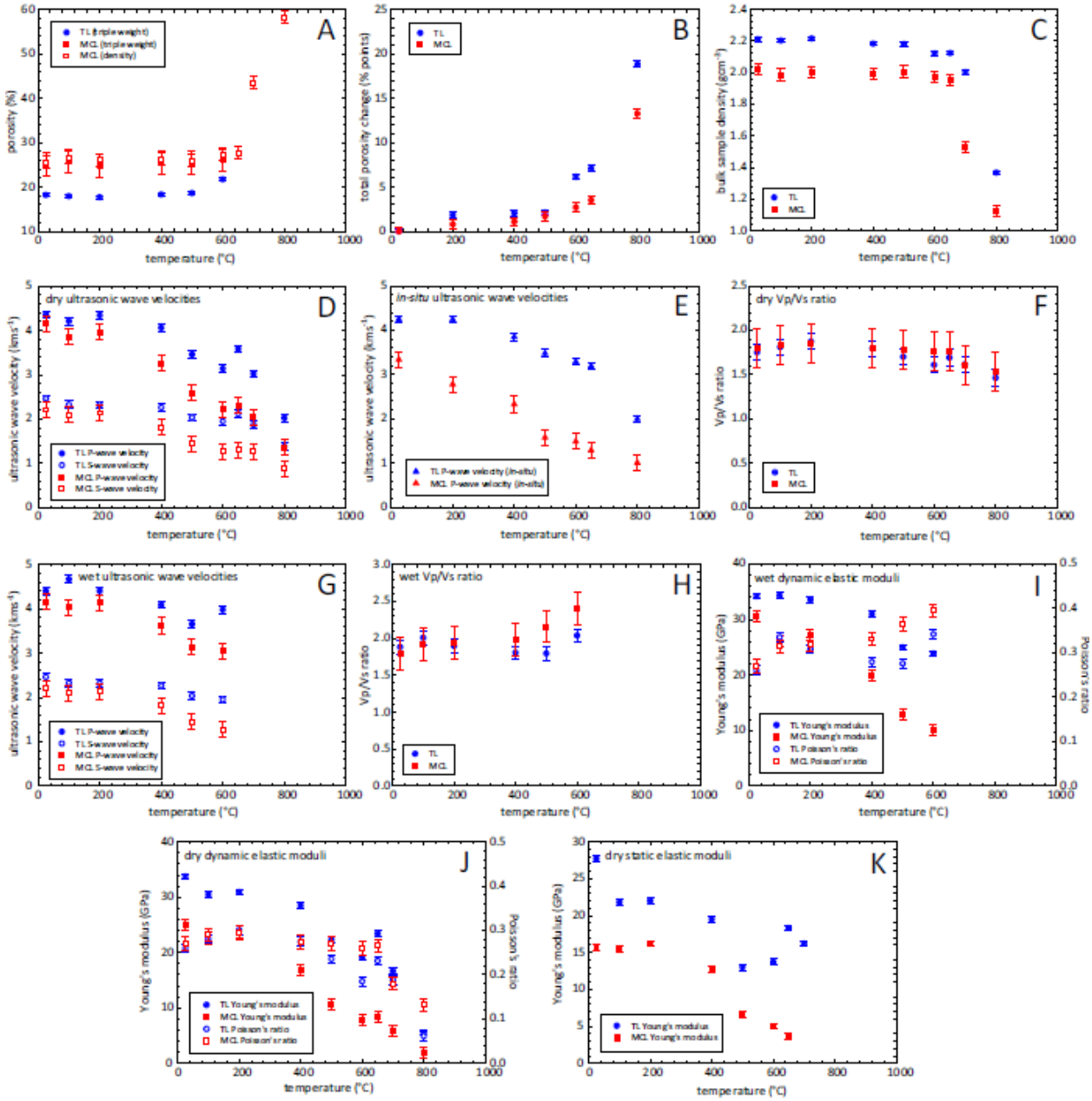

Fig. 10

ACCEPTED MANUSCRIPT

Research highlights

> High temperatures strongly influence sub-volcanic carbonate successions.

> Thermal weakening could encourage large-scale deformation at Mt. Etna.

> Geophysical anomalies/observations can be explained by such thermal degradation.

> Decarbonation should not be dismissed in CO_2 budgets for Mt. Etna.

> Carbonate basements may emerge as a decisive fundamental in volcanic stability.

ACCEPTED MANUSCRIPT